

---

# Beyond Isotropy in JEPAs: Hamiltonian Geometry and Symplectic Prediction

---

Robert Jenkinson Alvarez

3 March 2026

## Abstract

JEPAs often regularize one-view embeddings toward an isotropic Gaussian, implicitly baking Euclidean symmetry into the representation. We show that this is not merely a benign default. For a known structured downstream geometry  $H \succ 0$ , the minimax and maximum-entropy covariance under a Hamiltonian energy budget is  $(c/d)H^{-1}$ , and Euclidean isotropy incurs a closed-form price of isotropy. More importantly, when the downstream geometry is unknown, no geometry-independent fixed marginal target is canonical: every fixed covariance shape can be maximally misaligned for some structured geometry. We further show that even oracle one-view marginals do not identify the JEPA view-to-view predictive coupling. These results suggest that the structural bias in JEPAs should enter the cross-view coupling rather than a fixed encoder marginal. We instantiate this principle with **HamJEPa**, which encodes each view as a phase-space state  $(q, p)$  and predicts view-to-view transitions with a learned Hamiltonian leapfrog map, while non-isotropic scale and spectral floors prevent collapse. In a deliberately headless token protocol, HamJEPa improves over SIGReg on CIFAR-100 by +4.89 kNN@20 and +3.52 linear-probe points at 30 epochs, and by +6.45 kNN@20 and +10.64 linear-probe points at 80 epochs, while a matched MLP predictor ablation shows that the symplectic coupling is the ingredient driving the neighborhood-geometry gain. On ImageNet-100, HamJEPa- $q$  improves by +4.82 kNN@20 and +7.52 linear-probe points at 45 epochs.

## 1 Introduction

Joint Embedding Predictive Architectures (JEPAs) learn representations by predicting one embedding from another. For a fixed predictive loss, downstream performance depends on embedding geometry: scale, anisotropy, and collapse. We study objectives of the form  $\min_{\theta} \mathcal{L}_{\text{JEPa}}(\theta) + \lambda \mathcal{L}_{\text{reg}}(Z_{\theta})$ , where  $\mathcal{L}_{\text{reg}}$  regularizes the embedding distribution induced by the encoder.

A standard target is an *isotropic Gaussian* embedding distribution. LeJEPa motivates this choice under a “no downstream structure” viewpoint and enforces it with Sketched Isotropic Gaussian Regularization (SIGReg) [3]. Isotropy is a symmetry assumption: it treats all embedding directions as exchangeable. In many settings (patch-token grids, sequences, graphs), the index set carries known structure that induces preferred correlations and invariances; enforcing Euclidean isotropy can misalign the representation with this geometry.

This paper makes three linked contributions. First, for a fixed structured downstream geometry  $H$ , we derive the minimax and maximum-entropy covariance  $(c/d)H^{-1}$  and the price paid by Euclidean isotropy. Second, we show that this oracle result should not be interpreted as a new universal marginal target: when  $H$  is unknown, no geometry-independent fixed covariance shape is canonical, and even oracle marginals do not identify predictive coupling. Third, we instantiate the resulting design principle with a phase-space JEPa (*HamJEPa*) that places Hamiltonian structure in the cross-view predictor through a symplectic leapfrog map while using non-isotropic scale and spectral floors to prevent collapse.

Code and models: GitHub: HamJEPa-HamSIGReg.

### 1.1 Positioning relative to prior regularizers and dynamics priors

LeJEPa regularizes Euclidean embeddings toward an isotropic Gaussian using SIGReg, a sliced characteristic-function (CF) matching objective [3]. KerJEPa broadens this marginal-discrepancy viewpoint with kernel-based discrepancies [22]. HamJEPa departs from this line by asking when Euclidean isotropy is misaligned with structured task geometry and by placing Hamiltonian structure in the predictive map rather than prescribing a Euclidean-isotropic encoder marginal.

Several SSL objectives prevent collapse through low-order or spectral statistics, including Barlow Twins, VICReg, MCR<sup>2</sup>, and coding-rate-regularized self-distillation [4, 18–20]. HamJEPa uses related scale and spectral non-degeneracy controls, but couples them to a phase-space JEPa with a symplectic predictor; we do not claim these anti-collapse penalties are novel in isolation.

Hamiltonian Neural Networks, Hamiltonian Generative Networks, and Symplectic ODE-Net impose energy-based or symplectic structure on learned dynamics, typically for temporal or control data [8, 15, 21]. HamJEPa uses the same geometric bias in a different role: a predictor prior for paired augmentations, not a physics model of observed trajectories.

## 2 Setup

**Data, views, and randomness.** Let  $x \sim \mathcal{D}$  be a data sample and let  $\tau \sim \mathcal{A}$  be a random augmentation. A *view* is  $v := \tau(x)$ . We sample paired views of the same sample:

$$v_a = \tau_a(x), \quad v_b = \tau_b(x). \quad (1)$$

We use two representation parameterizations:

(A) *Euclidean embedding.* An encoder  $f_\theta : \mathcal{X} \rightarrow \mathbb{R}^d$  maps a view to an embedding random variable

$$Z := f_\theta(V) \in \mathbb{R}^d, \quad (2)$$

where  $V$  denotes a generic random view. Assume finite second moments. Let  $\mu_\theta := \mathbb{E}[Z]$  and  $\Sigma_\theta := \text{Cov}(Z) \succeq 0$ . We write centered embeddings as  $\tilde{Z} := Z - \mu_\theta$  so  $\mathbb{E}[\tilde{Z}] = 0$  and  $\text{Cov}(\tilde{Z}) = \Sigma_\theta$ .

(B) *Phase-space state (HamJEPa).* A phase-space encoder  $E_\theta : \mathcal{X} \rightarrow \mathbb{R}^{2d_0}$  outputs a state

$$S := E_\theta(V) = (Q, P), \quad Q, P \in \mathbb{R}^{d_0}. \quad (3)$$

We interpret  $Q$  as a *content* coordinate and  $P$  as an auxiliary *momentum* coordinate used to model structured view-to-view transitions. We write projections  $\pi_q(Q, P) = Q$  and  $\pi_p(Q, P) = P$ .

**Batch (row) convention.** For a minibatch of size  $n$ , we stack embeddings/states as row vectors:  $\mathbf{Z} \in \mathbb{R}^{n \times d}$  has rows  $z_i^\top$ , and  $\mathbf{S} \in \mathbb{R}^{n \times 2d_0}$  has rows  $s_i^\top = (q_i^\top, p_i^\top)$ . We center batches by subtracting the row-mean, e.g.  $\tilde{\mathbf{Z}} = \mathbf{Z} - \frac{1}{n} \mathbf{1} \mathbf{1}^\top \mathbf{Z}$ .

**Two Hamiltonians (to avoid notation collisions).** Section 3 uses an SPD operator  $H \succ 0$  to specify a *geometry* on embedding space. HamJEPa uses a *scalar energy*  $\mathcal{H}_\phi(q, p)$  generating a symplectic map on phase space. We reserve  $H$  for the SPD operator and  $\mathcal{H}_\phi$  for the scalar energy.

## 3 A Theory of Marginal Geometry and Predictive Coupling in JEPAs

This section is pure theory: given a structured notion of task complexity and an energy budget, what covariance/distribution is canonical, and what is the cost of forcing Euclidean isotropy? Throughout this section, fix an SPD operator  $H \succ 0$ , which defines the structured embedding geometry through the quadratic energy  $z^\top H z$ ; Hamiltonian-isotropic covariance in this geometry has the form  $\alpha H^{-1}$ . We work with the centered embedding  $\tilde{Z} := Z - \mathbb{E}[Z]$  and write  $\Sigma := \text{Cov}(\tilde{Z})$ .

### 3.1 Setup: structured tasks and a Hamiltonian budget

We model downstream *linear* tasks by  $y = w^\top \tilde{Z}$  and constrain task complexity by the  $H^{-1}$ -unit ball

$$\mathcal{W}_H := \{w \in \mathbb{R}^d : w^\top H^{-1} w \leq 1\}. \quad (4)$$

We pair this with a representation energy budget in the  $H$ -geometry:

$$\mathbb{E}[\tilde{Z}^\top H \tilde{Z}] = \text{tr}(H\Sigma) = c, \quad c > 0. \quad (5)$$

Given  $\Sigma \succeq 0$ , define the worst-case task variance functional

$$V(\Sigma) := \sup_{w \in \mathcal{W}_H} w^\top \Sigma w. \quad (6)$$

The next lemma gives a convenient spectral form.

**Lemma 3.1** (Spectral form of  $V(\Sigma)$ ). *For any  $\Sigma \succeq 0$ ,*

$$V(\Sigma) = \lambda_{\max}(H^{1/2} \Sigma H^{1/2}). \quad (7)$$

*Moreover, if  $u_{\max}$  is a unit top eigenvector of  $H^{1/2} \Sigma H^{1/2}$ , then  $w_{\max} := H^{1/2} u_{\max}$  attains the supremum in (6).*

*Proof.* See Appendix B.1.1. □

### 3.2 Minimax covariance under a Hamiltonian budget

We ask for the covariance that minimizes the worst-case task variance (6) under the  $H$ -budget (5).

**Theorem 3.2** (Minimax covariance under a Hamiltonian budget). *Fix  $H \succ 0$  and  $c > 0$ . Consider*

$$\min_{\Sigma \succeq 0: \text{tr}(H\Sigma) = c} V(\Sigma). \quad (8)$$

*The unique minimizer is*

$$\Sigma^* = \frac{c}{d} H^{-1}, \quad (9)$$

*and the optimal value is*

$$\min_{\Sigma \succeq 0: \text{tr}(H\Sigma) = c} V(\Sigma) = \frac{c}{d}. \quad (10)$$

*Equivalently,  $H^{1/2} \Sigma^* H^{1/2} = \frac{c}{d} I$ .*

*Proof.* See Appendix B.1.2. □

### 3.3 Maximum entropy: the canonical distribution

The minimax result selects a canonical covariance. A complementary principle selects a canonical *distribution*.

**Theorem 3.3** (Maximum entropy under a Hamiltonian energy constraint). *Let  $Z$  be an  $\mathbb{R}^d$ -valued random vector with a density,  $\mathbb{E}[Z] = 0$ , and finite second moments. Among all such distributions satisfying*

$$\mathbb{E}[Z^\top H Z] = c, \quad (11)$$

*the unique maximizer of differential entropy is the Gaussian*

$$Z \sim \mathcal{N}\left(0, \frac{c}{d} H^{-1}\right). \quad (12)$$

*Proof.* See Appendix B.1.3. □

### 3.4 Price of Euclidean isotropy

Many practical objectives encourage Euclidean isotropy, i.e.,  $\Sigma \propto I$  in the original coordinates. This subsection quantifies the worst-case gap incurred by imposing Euclidean isotropy under the same Hamiltonian budget.

Under the restriction  $\Sigma = \sigma^2 I$ , the constraint  $\text{tr}(H\Sigma) = c$  forces the unique feasible Euclidean-isotropic covariance

$$\Sigma_{\text{iso}} = \frac{c}{\text{tr}(H)} I. \quad (13)$$

**Theorem 3.4** (Price of Euclidean isotropy). *Fix  $H \succ 0$  and  $c > 0$ . Let  $\Sigma^*$  be as in Theorem 3.2 and let  $\Sigma_{\text{iso}}$  be as in (13). Then*

$$V(\Sigma_{\text{iso}}) = \frac{c}{\text{tr}(H)} \lambda_{\max}(H), \quad (14)$$

$$\frac{V(\Sigma_{\text{iso}})}{V(\Sigma^*)} = \rho(H) := \frac{d \lambda_{\max}(H)}{\text{tr}(H)}. \quad (15)$$

Moreover  $1 \leq \rho(H) \leq d$ , with  $\rho(H) = 1$  if and only if  $H \propto I$ .

*Proof.* See Appendix B.1.4. □

**Proposition 3.5** (Metric isotropy equivalence). *Let  $H \succ 0$  and let  $Z \in \mathbb{R}^d$  be a random vector with finite second moments and covariance  $\Sigma := \text{Cov}(Z)$ . Define the  $H$ -whitened representation  $Z' := H^{1/2}Z$ . Then*

$$\text{Cov}(Z') = H^{1/2} \Sigma H^{1/2}.$$

In particular, for any  $\alpha > 0$ ,

$$\Sigma = \alpha H^{-1} \iff \text{Cov}(Z') = \alpha I.$$

*Proof.* See Appendix B.1.5. □

### 3.5 A quadratic Hamiltonian lift of the oracle structured Gaussian

The structured Gaussian selected by Theorems 3.2 and 3.3 admits a natural lift to a Gibbs law on phase space.

**Proposition 3.6** (Quadratic Hamiltonian lift of the oracle covariance). *Fix  $H \succ 0$  and  $c > 0$ , and define the quadratic Hamiltonian*

$$\mathcal{H}_H(q, p) := \frac{1}{2} q^\top H q + \frac{1}{2} \|p\|_2^2, \quad q, p \in \mathbb{R}^d. \quad (16)$$

Consider the Gibbs density on phase space

$$\pi_H(q, p) \propto \exp\left(-\frac{d}{c} \mathcal{H}_H(q, p)\right). \quad (17)$$

Then  $q$  and  $p$  are independent under  $\pi_H$ , with

$$q \sim \mathcal{N}\left(0, \frac{c}{d} H^{-1}\right), \quad p \sim \mathcal{N}\left(0, \frac{c}{d} I\right). \quad (18)$$

Moreover,

$$\mathbb{E}_{\pi_H}[q^\top H q] = c, \quad \mathbb{E}_{\pi_H}[\|p\|_2^2] = c, \quad \mathbb{E}_{\pi_H}[\mathcal{H}_H(q, p)] = c. \quad (19)$$

In particular, the  $q$ -marginal of  $\pi_H$  is exactly the minimax-optimal and maximum-entropy law from Theorems 3.2 and 3.3.

*Proof.* See Appendix B.1.6. □

**Proposition 3.7** (The oracle family spans the SPD cone). *Fix  $c > 0$ . As  $H$  ranges over SPD operators, the family*

$$\Sigma^*(H) = \frac{c}{d} H^{-1} \quad (20)$$

ranges over the entire SPD cone. Equivalently, for every  $\Sigma \succ 0$ , choosing

$$H = \frac{c}{d} \Sigma^{-1} \quad (21)$$

yields  $\Sigma^*(H) = \Sigma$ .

*Proof.* See Appendix B.1.7. □

**From the oracle covariance to a practical unknown- $H$  relaxation.** Proposition 3.6 shows that when  $H$  is known, the oracle covariance  $\Sigma^* = \frac{c}{d}H^{-1}$  is exactly the  $q$ -marginal of a quadratic Hamiltonian Gibbs model on phase space. In that quadratic oracle case, the induced dynamics are

$$\dot{q} = p, \quad \dot{p} = -Hq, \quad (22)$$

so a Hamiltonian predictor is not an unrelated construction, but a natural dynamical realization of the same structured geometry.

This does *not* mean that the practical training mechanism is uniquely determined by Section 3. Rather, the theory should be read as an oracle statement: when  $H$  is known, the correct geometry is Hamiltonian-anisotropic rather than Euclidean-isotropic. When  $H$  is unknown, Proposition 3.7 shows that the oracle family  $\{\Sigma^*(H) : H \succ 0\}$  spans the entire SPD cone, so the theory no longer singles out one fixed covariance target.

**Why not learn another fixed marginal target?** The previous results might suggest replacing Euclidean isotropy by a better fixed target covariance. The next result shows why this is brittle when downstream geometry is unknown.

**Theorem 3.8** (No universal fixed marginal target). *Fix any SPD target shape  $M \succ 0$  independent of the downstream geometry. Under geometry  $H \succ 0$ , the budget-feasible covariance with shape  $M$  is*

$$\Sigma_M(H) := \frac{c}{\text{tr}(HM)} M.$$

*Its regret relative to the oracle covariance  $\Sigma^*(H) = (c/d)H^{-1}$  is*

$$\frac{V_H(\Sigma_M(H))}{V_H(\Sigma^*(H))} = \frac{d \lambda_{\max}(H^{1/2} M H^{1/2})}{\text{tr}(HM)}.$$

*This quantity equals 1 iff  $M \propto H^{-1}$ , and for every fixed  $M \succ 0$ ,*

$$\sup_{H \succ 0} \frac{V_H(\Sigma_M(H))}{V_H(\Sigma^*(H))} = d.$$

*Thus no geometry-independent fixed covariance shape is canonical for all structured downstream geometries.*

*Proof.* See Appendix B.1.8. □

**Proposition 3.9** (Oracle marginals do not identify the predictive coupling). *Let  $Z_a, Z_b \in \mathbb{R}^d$  be centered jointly Gaussian random vectors with  $\text{Cov}(Z_a) = \text{Cov}(Z_b) = \Sigma \succ 0$  and cross-covariance  $\text{Cov}(Z_b, Z_a) = C$ . Then*

$$\mathbb{E}[Z_b | Z_a] = C \Sigma^{-1} Z_a.$$

*Therefore, the same oracle marginal covariance  $\Sigma$  admits a continuum of different predictive maps as the admissible cross-covariance  $C$  varies. Marginal matching alone cannot determine the JEPA view-to-view prediction problem.*

*Proof.* See Appendix B.1.9. □

Together, Theorem 3.8 and Proposition 3.9 show that the unknown-geometry JEPA problem should not be reduced to choosing a single fixed encoder marginal. The structural bias must instead enter the view-to-view coupling. HamJEPA instantiates this principle by using a Hamiltonian phase-space coupling: the quadratic known- $H$  case recovers the oracle  $q$ -marginal, while the practical unknown- $H$  method uses a learned symplectic predictor and geometry-agnostic non-collapse constraints.

**Takeaway.** Section 3 does not merely say that Euclidean isotropy can be suboptimal. It shows that, under unknown downstream geometry, fixed marginal matching is the wrong object: no geometry-independent covariance target is universally canonical, and even an oracle marginal does not determine the JEPA predictive coupling. The structural bias must therefore enter the view-to-view map.

## 4 HamJEPa: Symplectic Predictive Structure Without Isotropic Marginals

Section 3 shows that fixed marginal matching is brittle under unknown structured geometry and that marginals alone do not determine JEPa prediction. HamJEPa therefore places the structural bias in the view-to-view coupling: a phase-space encoder is trained with a symplectic, volume-preserving predictor, while encoder-side scale and spectral constraints prevent collapse without enforcing isotropic Gaussian marginals. A visual overview of HamJEPa is provided in Appendix E.

### 4.1 Phase-space encoder

Given paired views  $v_a, v_b$  as defined in Section 2, the encoder  $E_\theta : \mathcal{X} \rightarrow \mathbb{R}^{2d_0}$  outputs phase-space states  $s_a = E_\theta(v_a)$  and  $s_b = E_\theta(v_b)$  with  $s = (q, p) \in \mathbb{R}^{2d_0}$ .

$$s = E_\theta(v) = (q, p), \quad q, p \in \mathbb{R}^{d_0}. \quad (23)$$

We interpret  $q$  as a *content* coordinate used for prediction and evaluation, and  $p$  as an auxiliary *momentum* coordinate enabling structured transitions. We write  $\pi_q(q, p) = q$  and  $\pi_p(q, p) = p$ .

**Observable coordinate vs. conjugate latent.** Section 3 is formulated in terms of the representation used by downstream tasks; in HamJEPa, that conceptual role is played by  $q$ . The auxiliary coordinate  $p$  is the conjugate latent that makes Hamiltonian transport possible. For non-invertible augmentations, this makes  $q$ -matching the cleanest observable formulation, since the target need not contain a uniquely recoverable dynamical state. In practice, however, the exact matching choice is a stability knob rather than a theorem: on CIFAR-100 we primarily use  $q$ -matching, while on ImageNet-100 we found full-state  $(q, p)$ -matching more stable and therefore use it there.

### 4.2 Symplectic predictor via a separable Hamiltonian and leapfrog

**Canonical symplectic structure.** Let

$$J := \begin{pmatrix} 0 & I \\ -I & 0 \end{pmatrix} \in \mathbb{R}^{2d_0 \times 2d_0} \quad (24)$$

denote the canonical symplectic matrix.

**Hamilton’s equations and flow map.** Given a differentiable scalar energy  $\mathcal{H}_\phi : \mathbb{R}^{2d_0} \rightarrow \mathbb{R}$ , Hamilton’s ODE on phase space is

$$\dot{s}(t) = J \nabla_s \mathcal{H}_\phi(s(t)), \quad s(0) = s_0, \quad (25)$$

where  $J$  is the canonical symplectic matrix (24). We denote its time- $t$  flow map by  $\Phi_{\phi, t}$ , i.e.  $s(t) = \Phi_{\phi, t}(s_0)$ .

**Separable energy (the theory-tight choice).** To obtain a discrete predictor map with rigorous symplectic guarantees under an explicit integrator, we use a separable Hamiltonian energy

$$\mathcal{H}_\phi(q, p) = T(p) + V_\phi(q), \quad T(p) = \frac{1}{2} \|p\|_2^2, \quad (26)$$

where  $V_\phi : \mathbb{R}^{d_0} \rightarrow \mathbb{R}$  is a learnable potential. Fixing  $T(p) = \frac{1}{2} \|p\|_2^2$  is stabilizing and prevents scale-control constraints from being satisfied by rescaling a learnable kinetic metric.

**Leapfrog (velocity Verlet) predictor map.** Given step size  $\Delta t > 0$  and  $K \in \mathbb{N}$  steps, define the leapfrog update

$$\begin{aligned} p_{k+\frac{1}{2}} &= p_k - \frac{\Delta t}{2} \nabla_q V_\phi(q_k), \\ q_{k+1} &= q_k + \Delta t p_{k+\frac{1}{2}}, & k &= 0, \dots, K-1. \\ p_{k+1} &= p_{k+\frac{1}{2}} - \frac{\Delta t}{2} \nabla_q V_\phi(q_{k+1}), \end{aligned} \quad (27)$$

This defines a one-step map  $\Psi_{\phi, \Delta t} : \mathbb{R}^{2d_0} \rightarrow \mathbb{R}^{2d_0}$  and a  $K$ -step predictor

$$\Phi_\phi^{(K)} := \Psi_{\phi, \Delta t}^K. \quad (28)$$

Given  $s_a = (q_a, p_a)$ , we predict  $\hat{s}_b = (\hat{q}_b, \hat{p}_b)$  by

$$\hat{s}_b = \Phi_\phi^{(K)}(s_a). \quad (29)$$

### 4.3 Objective: content prediction plus non-isotropic anti-collapse

The projected log-det and participation-ratio penalties should be understood as an encoder-side anti-collapse bridge, not as the primary novelty of the method; similar covariance-volume objectives appear elsewhere, whereas our contribution is to couple such non-collapse controls with a phase-space JEPA and a symplectic predictive prior.

Let  $s_a = (q_a, p_a) = E_\theta(v_a)$ ,  $s_b = (q_b, p_b) = E_\theta(v_b)$ , and  $\hat{s}_b = (\hat{q}_b, \hat{p}_b) = \Phi_\phi^{(K)}(s_a)$ . HamJEPA optimizes

$$\min_{\theta, \phi} \mathcal{L}_{\text{pred}} + \lambda_{\text{bi}} \mathcal{L}_{\text{bi}} + \lambda_{\text{budget}} \mathcal{L}_{\text{budget}} + \lambda_{\text{vol}} \mathcal{L}_{\text{vol}} + \lambda_{\text{pr}} \mathcal{L}_{\text{pr}} + \lambda_{\text{wd}} \mathcal{R}_{\text{wd}}(\theta, \phi). \quad (30)$$

All expectations are implemented as minibatch averages;  $\text{sg}(\cdot)$  denotes stop-gradient.

**(1) Matching loss.** Let  $m \in \{q, qp\}$  denote the matching mode, with  $\Pi_q(q, p) = q$  and  $\Pi_{qp}(q, p) = (q, p)$ . CIFAR-100 uses  $m = q$ , while ImageNet-100 uses  $m = qp$  for stability. We define

$$\mathcal{L}_{\text{pred}} := \mathbb{E}[\|\Pi_m(\hat{s}_b) - \text{sg}(\Pi_m(s_b))\|_2^2]. \quad (31)$$

**(2) Bidirectional prediction.** Define the backward prediction by running the *same* integrator with step size  $-\Delta t$ :

$$\hat{s}_a = \Phi_\phi^{(K)}(s_b; -\Delta t).$$

The bidirectional loss is

$$\mathcal{L}_{\text{bi}} := \mathbb{E}[\|\pi_q(\Phi_\phi^{(K)}(s_a; +\Delta t)) - \text{sg}(q_b)\|_2^2 + \|\pi_q(\Phi_\phi^{(K)}(s_b; -\Delta t)) - \text{sg}(q_a)\|_2^2]. \quad (32)$$

Time reversibility of leapfrog (Corollary A.5) makes this an “exact inverse in-model” constraint rather than an independent predictor.

**(3) Fixed-units scale budget (anti-gauge).** Symplecticity constrains the predictor map but does not prevent the encoder from collapsing all views to a point. We therefore enforce scale budgets in fixed units (no Gaussianity, no isotropy):

$$\mathcal{L}_{\text{budget}} := \left( \frac{\mathbb{E}\|q\|_2^2}{d_0} - \alpha_q \right)^2 + \left( \frac{\mathbb{E}\|p\|_2^2}{d_0} - \alpha_p \right)^2, \alpha_q, \alpha_p > 0. \quad (33)$$

**(4) Projected log-det volume floor.** A scale budget alone can be satisfied by concentrating variance in a low-dimensional subspace. To prevent rank collapse without forcing isotropy, we impose a projected log-det floor on the content batch. Let  $Q \in \mathbb{R}^{B \times d_0}$  contain centered content codes:  $Q_i = q_i - \frac{1}{B} \sum_{j=1}^B q_j$ . Sample a random projection  $R \in \mathbb{R}^{d_0 \times k}$  with orthonormalized columns ( $k \ll d_0$ ) and form  $Y = QR \in \mathbb{R}^{B \times k}$ . Define the regularized projected covariance

$$\Sigma_Y := \frac{1}{B-1} Y^\top Y + \varepsilon I_k, \quad \varepsilon > 0, \quad (34)$$

and per-dimension log-volume

$$\ell_{\text{vol}} := \frac{1}{k} \log \det(\Sigma_Y). \quad (35)$$

We use the hinge penalty

$$\mathcal{L}_{\text{vol}} := [\max(0, \tau - \ell_{\text{vol}})]^2, \quad \tau \in \mathbb{R}. \quad (36)$$

**(5) Participation ratio floor (prevents “one-spike” solutions).** Log-det alone can be satisfied with one very large eigenvalue and many tiny ones when scale is not tightly controlled, or when minibatch effects dominate. To explicitly rule out the “one-spike” regime, we add a participation ratio (PR) floor on  $\Sigma_Y$ :

$$\text{PR}(\Sigma_Y) := \frac{(\text{tr}(\Sigma_Y))^2}{\text{tr}(\Sigma_Y^2)} = \frac{(\sum_{i=1}^k \lambda_i)^2}{\sum_{i=1}^k \lambda_i^2} \in [1, k], \quad (37)$$

where  $\lambda_1, \dots, \lambda_k$  are the eigenvalues of  $\Sigma_Y$ . We penalize violations of a target effective rank  $r_0 \in (1, k]$ :

$$\mathcal{L}_{\text{pr}} := [\max(0, r_0 - \text{PR}(\Sigma_Y))]^2. \quad (38)$$

Together, these terms prevent collapse while permitting anisotropy; *HamJEPA* does not constrain representations to a unit sphere or isotropic Gaussian target.

## 4.4 Structural guarantees

The formal structural theory of HamJEPa is deferred to Appendix A. At a high level, the separable Hamiltonian (26) and leapfrog update (27) imply that the  $K$ -step predictor  $\Phi_\phi^{(K)}$  is symplectic:

$$(D\Phi_\phi^{(K)}(s))^\top J(D\Phi_\phi^{(K)}(s)) = J, \quad \det D\Phi_\phi^{(K)}(s) = 1. \quad (39)$$

Thus the predictor is locally volume-preserving and is inverted by running leapfrog with step size  $-\Delta t$ . Since symplecticity constrains only the predictor, encoder collapse is controlled separately by the fixed-unit scale, projected log-det, and participation-ratio floors. Appendix A gives reciprocal singular-value pairing, shadow-Hamiltonian stability, and the anti-collapse lemmas.

## 5 Results

**Controlled protocol.** We evaluate frozen representations on CIFAR-100 and ImageNet-100 using cosine  $k$ NN and linear probing. The goal is not a projector-heavy SOTA recipe, but an objective-level comparison: all methods share the same backbone, augmentations, optimizer, batch size, schedule, two global views, no local views, the encoder runs in a headless token regime using ResNet stage-3 (layer3) features, and identity projector. For HamJEPa, the encoder output  $s = (q, p)$  is split channel-wise;  $q$  is the primary readout, while  $p$  and  $(q, p)$  test auxiliary-state and dimension effects. Full details and diagnostics are in Appendix D–F. SIGReg is the isotropic-Gaussian JEPa baseline closest to our theoretical comparison. This protocol is intentionally underpowered by modern SSL standards. By removing projection heads, local crops, EMA teachers, and recipe-specific tuning, the comparison isolates whether changing the predictive geometry changes the frozen representation.

### 5.1 CIFAR-100: controlled gains and predictor ablation

HamJEPa improves over SIGReg after only 30 epochs under the same backbone, views, optimizer, and identity projector. Using the primary  $q$  readout, HamJEPa gains +4.89 points in  $k$ NN@20 (31.45 vs. 26.56) and +3.52 points in linear probing (33.95 vs. 30.43). The  $p$  readout is also predictive (29.71  $k$ NN@20; 33.07 linear), but remains behind  $q$  in nearest-neighbor accuracy, matching the intended role of  $q$  as the content coordinate and  $p$  as an auxiliary dynamical coordinate. Concatenating  $(q, p)$  gives the strongest linear probe at 30 epochs (34.18), while  $q$  alone gives the strongest  $k$ NN geometry.

The 80-epoch predictor-family ablation gives the sharper control. MLP-HJEPa keeps the phase-space encoder, channel-wise  $q/p$  split, identity projector, prediction loss, anti-collapse regularizers, optimizer, batch size, and training schedule fixed, and replaces only the symplectic leapfrog map with a non-symplectic residual MLP predictor. This ablation is intentionally strong: MLP-HJEPa reaches high linear accuracy (42.26–42.77), showing that the phase-space split and regularizers can produce linearly useful features. However, its  $k$ NN@20 accuracy remains essentially at the SIGReg level (28.10–28.30 vs. 27.98). By contrast, HamJEPa with the symplectic predictor reaches 34.43  $k$ NN@20 and 44.59 linear accuracy using the  $q$  readout. Thus the main geometric gain is not explained by the  $q/p$  split, anti-collapse terms, or generic MLP capacity: replacing the MLP by a symplectic Hamiltonian predictor yields a +6.33 point  $k$ NN@20 gain over MLP-HJEPa- $q$  and a +6.45 point gain over SIGReg at the same 80-epoch budget.

### 5.2 ImageNet-100: same minimal recipe, larger-scale signal

On ImageNet-100, HamJEPa again improves over SIGReg under the same minimal recipe (45 epochs, single seed). Using the primary  $q$  readout, HamJEPa gains +4.82 points in  $k$ NN@20 (24.92 vs. 20.10) and +7.52 points in linear probing (31.92 vs. 24.40). The best HamJEPa linear readout is  $p$  at 32.08, giving a +7.68 point gain over SIGReg- $q$ . These gains are not explained by feature dimension. SIGReg benefits modestly from concatenating its two 1024-d blocks:  $q \rightarrow (q, p)$  improves by +0.84  $k$ NN@20 points (20.10  $\rightarrow$  20.94) and +1.14 linear-probe points (24.40  $\rightarrow$  25.54). In contrast, HamJEPa gains essentially nothing from concatenation in  $k$ NN (24.92  $\rightarrow$  24.64) and only +0.12 in linear probing (31.92  $\rightarrow$  32.04). Crucially, the 1024-d HamJEPa- $q$  readout already outperforms the 2048-d SIGReg- $(q, p)$  readout by +3.98 points in  $k$ NN@20 and +6.38 points in linear probing.

We match the full phase space  $(q, p)$  during pretraining for stability. Consistent with this objective,  $p$  is highly predictive and slightly exceeds  $q$  on the linear probe (32.08 vs. 31.92), while remaining

Setting	Method / readout	$k$ NN@20 (%)	Linear (%)	$k$ NN best (%)
<i>30 epochs, mean±std over 3 seeds</i>				
	SIGReg	26.56 ± 0.18	30.43 ± 0.30	–
	HamJEPA- $q$	<b>31.45 ± 0.27</b>	33.95 ± 0.24	–
	HamJEPA- $p$	29.71 ± 0.25	33.07 ± 0.36	–
	HamJEPA- $(q, p)$	30.88 ± 0.39	<b>34.18 ± 0.17</b>	–
<i>80 epochs, predictor-family ablation</i>				
	SIGReg	27.98	33.95	28.71 @ $k=1$
	MLP-HJEPA- $q$	28.10	42.26	28.10 @ $k=20$
	MLP-HJEPA- $p$	28.30	41.90	28.30 @ $k=20$
	MLP-HJEPA- $(q, p)$	28.15	42.77	28.15 @ $k=20$
	HamJEPA- $q$	<b>34.43</b>	<b>44.59</b>	<b>34.43 @ <math>k=20</math></b>
	HamJEPA- $p$	32.96	44.44	32.96 @ $k=20$
	HamJEPA- $(q, p)$	33.66	44.52	33.66 @ $k=20$

Table 1: **CIFAR-100 controlled results.** The 30-epoch block shows short-budget performance; the 80-epoch block isolates the predictor family. MLP-HJEPA differs from HamJEPA only by replacing the symplectic leapfrog predictor with a non-symplectic residual MLP.

Method	$k$ NN@20 (%)	Linear probe (%)
SIGReg ( $q$ -eval)	20.10	24.40
SIGReg ( $p$ -eval)	18.78	23.86
SIGReg ( $(q, p)$ -eval)	20.94	25.54
HamJEPA ( $q$ -eval)	<b>24.92</b>	31.92
HamJEPA ( $p$ -eval)	24.72	<b>32.08</b>
HamJEPA ( $(q, p)$ -eval)	24.64	32.04

Table 2: **ImageNet-100 downstream performance after 45 epochs** of pretraining, single seed. For HamJEPA,  $q$  and  $p$  are learned phase-space coordinates. For SIGReg, the same split is a representation-block / dimension control rather than a literal position–momentum decomposition.

comparable in  $k$ NN (24.72 vs. 24.92). However, concatenating  $(q, p)$  does not improve  $k$ NN, suggesting that the nearest-neighbor geometry is not simply a consequence of evaluating a larger vector. The result is therefore a controlled objective-level delta: HamJEPA improves frozen-feature geometry in a deliberately headless setting where neither projection-head capacity nor representation dimension explains the gain.

**Geometry diagnostics.** The accuracy gains are accompanied by broader, non-collapsed covariance spectra without enforcing an isotropic Gaussian marginal. On ImageNet-100, SIGReg- $q$  has effective rank  $\approx 38.33$  and PR  $\approx 24.91$ , while HamJEPA- $q$  reaches  $\approx 94.73$  and  $\approx 45.27$ ; even the larger SIGReg- $(q, p)$  representation remains lower ( $\approx 51.16$  and  $\approx 36.17$ ). CIFAR-100 shows the same qualitative pattern, with HamJEPA- $q$  increasing effective rank from  $\approx 109.7$  to  $\approx 124.5$ . Full spectra and training-time diagnostics are deferred to Appendix D.

## 6 Conclusion

We showed that Euclidean-isotropic JEPA regularization can be misaligned with structured task geometry, and that fixed marginal targets are brittle when the downstream geometry is unknown. HamJEPA instead places Hamiltonian structure in the view-to-view predictor: views are encoded as phase-space states, predicted with a symplectic leapfrog map, and kept non-collapsed by non-isotropic scale and spectral floors. Under a deliberately headless token protocol, HamJEPA improves frozen-feature  $k$ NN and linear-probe performance over SIGReg on CIFAR-100 and ImageNet-100.

**Limitations.** This is a controlled geometry study rather than a SOTA SSL recipe. The main baseline is SIGReg. ImageNet-100 is single-seed, and we do not learn or recover the downstream operator  $H$ ; broader baselines, multi-seed ImageNet runs, and learned structured geometries remain future work.

## References

- [1] Shun'ichi Amari. Differential-geometrical methods in statistics, 1985.
- [2] Mahmoud Assran, Quentin Duval, Ishan Misra, Piotr Bojanowski, Pascal Vincent, Michael Rabbat, Yann LeCun, and Nicolas Ballas. Self-supervised learning from images with a joint-embedding predictive architecture, 2023.
- [3] Randall Balestriero and Yann LeCun. Lejepa: Provable and scalable self-supervised learning without the heuristics, 2025. URL <https://arxiv.org/abs/2511.08544>.
- [4] Adrien Bardes, Jean Ponce, and Yann LeCun. Vicreg: Variance-invariance-covariance regularization for self-supervised learning, 2021.
- [5] Ludwig Boltzmann. Weitere studien über das wärmegleichgewicht unter gasmolekülen, 1872.
- [6] Ting Chen, Simon Kornblith, Mohammad Norouzi, and Geoffrey Hinton. A simple framework for contrastive learning of visual representations, 2020.
- [7] J. Willard Gibbs. Elementary principles in statistical mechanics: Developed with especial reference to the rational foundation of thermodynamics, 1902.
- [8] Sam Greydanus, Misko Dzamba, and Jason Yosinski. Hamiltonian neural networks, 2019. URL <https://arxiv.org/abs/1906.01563>.
- [9] Jean-Bastien Grill, Florian Strub, Florent Alché, Corentin Tallec, Pierre H. Richemond, Elena Buchatskaya, Carl Doersch, Bernardo Avila Pires, Zhaohan Daniel Guo, Mohammad Gheshlaghi Azar, Bilal Piot, Koray Kavukcuoglu, Rémi Munos, and Michal Valko. Bootstrap your own latent: A new approach to self-supervised learning, 2020.
- [10] William Rowan Hamilton. On a general method in dynamics, 1834.
- [11] E. T. Jaynes. Information theory and statistical mechanics, 1957.
- [12] Pierre-Simon Laplace. Traité de mécanique céleste, 1799.
- [13] Joseph Liouville. Sur la théorie de la variation des constantes arbitraires, 1838.
- [14] Siméon-Denis Poisson. Sur la variation des constantes arbitraires dans les questions de mécanique, 1809.
- [15] Peter Toth, Danilo Jimenez Rezende, Andrew Jaegle, Sébastien Racanière, Aleksandar Botev, and Irina Higgins. Hamiltonian generative networks, 2019.
- [16] Aäron van den Oord, Yazhe Li, and Oriol Vinyals. Representation learning with contrastive predictive coding, 2018.
- [17] Tongzhou Wang and Phillip Isola. Understanding contrastive representation learning through alignment and uniformity on the hypersphere, 2020.
- [18] Ziyang Wu, Jingyuan Zhang, Druv Pai, XuDong Wang, Chandan Singh, Jianwei Yang, Jianfeng Gao, and Yi Ma. Simplifying dino via coding rate regularization, 2025. URL <https://arxiv.org/abs/2502.10385>.
- [19] Yaodong Yu, Kwan Ho Ryan Chan, Chong You, Chaobing Song, and Yi Ma. Learning diverse and discriminative representations via the principle of maximal coding rate reduction. In *Advances in Neural Information Processing Systems*, volume 33, 2020.
- [20] Jure Zbontar, Li Jing, Ishan Misra, Yann LeCun, and Stéphane Deny. Barlow twins: Self-supervised learning via redundancy reduction, 2021.
- [21] Yaofeng Desmond Zhong, Biswadip Dey, and Amit Chakraborty. Symplectic ode-net: Learning hamiltonian dynamics with control, 2019.
- [22] Eric Zimmermann, Harley Wiltzer, Justin Szeto, David Alvarez-Melis, and Lester Mackey. Kerjepa: Kernel discrepancies for euclidean self-supervised learning, 2025. URL <https://arxiv.org/abs/2512.19605>.

## A Theory: symplecticity, volume preservation, and anti-collapse

This appendix records the structural guarantees enjoyed by HamJEPA when using the separable Hamiltonian (26) and the leapfrog integrator (27). These results justify the summary in Section 4.4: leapfrog gives a symplectic, volume-preserving, time-reversible predictor, while the encoder-side scale, log-det, and participation-ratio constraints prevent collapse without imposing Euclidean isotropic Gaussian marginals. All proofs are in Appendix B.2.

### A.1 Statements

**Row/column convention (linear transforms).** The paper uses column vectors for single states/embeddings and row-stacked matrices for minibatches. The following lemma formalizes the equivalence.

**Lemma A.1** (Row/column convention for left-multiplication by  $H^{1/2}$ ). *Let  $H \in \mathbb{R}^{d \times d}$  and let  $z \in \mathbb{R}^d$  be a column vector. Define  $z' := H^{1/2}z$ . Let  $\mathbf{Z} \in \mathbb{R}^{n \times d}$  be a row-stacked minibatch with rows  $\mathbf{Z}_{i,:} = z_i^\top$ . Define  $\mathbf{Z}' := \mathbf{Z}H^{1/2}$ . Then for every  $i$ ,*

$$(\mathbf{Z}')_{i,:}^\top = H^{1/2}z_i.$$

*Proof.* See Appendix B.2.1. □

**Symplecticity of the continuous flow.** We first state the standard symplecticity property of Hamiltonian flows.

**Theorem A.2** (Symplecticity of Hamiltonian flows). *Assume  $\mathcal{H}_\phi \in C^2(\mathbb{R}^{2d_0})$  and let  $\Phi_{\phi,t}$  denote the flow map of Hamilton's ODE (25). Then  $\Phi_{\phi,t}$  is symplectic: for all  $s$  and  $t$ ,*

$$(D\Phi_{\phi,t}(s))^\top J (D\Phi_{\phi,t}(s)) = J. \quad (40)$$

*Consequently,  $\det(D\Phi_{\phi,t}(s)) = 1$  for all  $s, t$ , and  $\Phi_{\phi,t}$  preserves phase-space volume (Liouville).*

*Proof.* See Appendix B.2.2. □

**Corollary A.3** (Volume-preserving maps preserve differential entropy). *Let  $F : \mathbb{R}^m \rightarrow \mathbb{R}^m$  be a  $C^1$  diffeomorphism and let  $X$  admit a density. Then*

$$h(F(X)) = h(X) + \mathbb{E}[\log |\det(DF(X))|].$$

*In particular, if  $|\det(DF(x))| = 1$  for all  $x$  (e.g.,  $F = \Phi_{\phi,t}$  from Theorem A.2), then  $h(F(X)) = h(X)$ .*

*Proof.* See Appendix B.2.3. □

**Symplecticity of the discrete predictor.** HamJEPA uses the leapfrog/Verlet map (27) as a discrete predictor. For separable Hamiltonians this map is symplectic.

**Theorem A.4** (Leapfrog is symplectic and volume-preserving for separable Hamiltonians). *Let  $\mathcal{H}_\phi(q, p) = T(p) + V_\phi(q)$  with  $T(p) = \frac{1}{2}\|p\|_2^2$  and  $V_\phi \in C^2$ . Then the one-step leapfrog map  $\Psi_{\phi,\Delta t}$  defined by (27) is symplectic. Therefore, for any  $K \geq 1$ , the  $K$ -step predictor  $\Phi_\phi^{(K)} = \Psi_{\phi,\Delta t}^K$  is symplectic and satisfies*

$$\det(D\Phi_\phi^{(K)}(s)) = 1 \quad \text{for all } s. \quad (41)$$

*Proof.* See Appendix B.2.4. □

**Corollary A.5** (Invertibility and time reversibility). *Under the assumptions of Theorem A.4, the leapfrog map is bijective and satisfies*

$$\Psi_{\phi,\Delta t}^{-1} = \Psi_{\phi,-\Delta t}. \quad (42)$$

*In particular, the  $K$ -step predictor admits an exact inverse by running the same integrator with step size  $-\Delta t$ :  $(\Phi_\phi^{(K)}(\cdot; +\Delta t))^{-1} = \Phi_\phi^{(K)}(\cdot; -\Delta t)$ .*

*Proof.* See Appendix B.2.5. □

**Proposition A.6** (Approximation of separable Hamiltonian flows by HamJEPA predictors). *Fix a horizon  $T > 0$  and a compact set  $K \subset \mathbb{R}^{2d_0}$ . Let  $K_q := \{q \in \mathbb{R}^{d_0} : \exists p \text{ with } (q, p) \in K\}$ .*

*Let  $V : \mathbb{R}^{d_0} \rightarrow \mathbb{R}$  be  $C^3$  on an open neighborhood of a compact set  $\Omega_q \supseteq K_q$ , and assume  $\nabla V$  is Lipschitz on  $\Omega_q$ . Let  $\Phi_t^V$  denote the time- $t$  flow map of Hamilton's ODE*

$$\dot{q} = p, \quad \dot{p} = -\nabla V(q)$$

*(i.e., the separable Hamiltonian  $H(q, p) = \frac{1}{2}\|p\|_2^2 + V(q)$ ).*

*For a learnable potential  $V_\phi \in C^3$  with  $\nabla V_\phi$  Lipschitz on  $\Omega_q$ , let  $\Psi_{\phi, \Delta t}$  be one leapfrog step (27) and let  $\Phi_\phi^{(K)} := \Psi_{\phi, \Delta t}^K$  with  $K\Delta t = T$  (28). Assume that for all initial states in  $K$ , both the exact trajectory under  $V$  and the exact trajectory under  $V_\phi$  remain inside  $\Omega := \Omega_q \times \Omega_p$  for all  $t \in [0, T]$ .*

*Then there exists a constant  $C = C(T, \Omega, V_\phi) > 0$  such that*

$$\sup_{(q,p) \in K} \|\Phi_\phi^{(K)}(q, p) - \Phi_T^V(q, p)\|_2 \leq C \left( \underbrace{\sup_{q \in \Omega_q} \|\nabla V_\phi(q) - \nabla V(q)\|_2}_{\text{modeling error}} + \underbrace{\Delta t^2}_{\text{integrator error}} \right).$$

*In particular, if the potential class can approximate  $\nabla V$  uniformly on  $\Omega_q$  (and admits bounded derivatives on  $\Omega_q$ ), then for every  $\varepsilon > 0$  there exist  $\phi$  and  $\Delta t > 0$  (hence  $K = T/\Delta t$ ) such that*

$$\sup_{(q,p) \in K} \|\Phi_\phi^{(K)}(q, p) - \Phi_T^V(q, p)\|_2 \leq \varepsilon.$$

*Proof.* See Appendix B.2.6. □

**Lemma A.7** (Reciprocal singular-value pairing). *Let  $A \in \mathbb{R}^{2d_0 \times 2d_0}$  be symplectic:  $A^\top J A = J$ . Then the singular values of  $A$  occur in reciprocal pairs: if  $\sigma$  is a singular value, so is  $1/\sigma$  (with the same multiplicity). Equivalently,  $A$  cannot be contractive in all directions; any local contraction must be compensated by expansion.*

*Proof.* See Appendix B.2.7. □

**Long-horizon stability (shadow Hamiltonians).** A core practical advantage of symplectic integrators is the existence of a nearby modified energy that explains stable multi-step rollouts. We record a standard backward-error-analysis statement.

**Theorem A.8** (Shadow Hamiltonian / backward error analysis (standard)). *Assume  $V_\phi$  is sufficiently smooth (e.g., analytic with bounded derivatives on the region visited by the numerical trajectory). Then for any integer  $N \geq 1$  there exists a modified Hamiltonian  $\tilde{\mathcal{H}}_{\phi, \Delta t}^{[N]}$  such that:*

1. **(Closeness)**  $\tilde{\mathcal{H}}_{\phi, \Delta t}^{[N]}(s) = \mathcal{H}_\phi(s) + \mathcal{O}(\Delta t^2)$  uniformly on the region of interest.
2. **(Modified-flow representation)** One leapfrog step equals the time- $\Delta t$  flow of  $\tilde{\mathcal{H}}_{\phi, \Delta t}^{[N]}$  up to local error  $\mathcal{O}(\Delta t^{N+1})$ .
3. **(Near-conservation)** Along the leapfrog iterates  $(s_k)$ , the modified energy  $\tilde{\mathcal{H}}_{\phi, \Delta t}^{[N]}(s_k)$  is nearly conserved, and the original energy error  $\mathcal{H}_\phi(s_k) - \mathcal{H}_\phi(s_0)$  remains bounded over long horizons when  $\Delta t$  is small.

*Proof* (sketch via BCH/backward error analysis). See Appendix B.2.8. □

**Anti-collapse: what each ingredient does (and does not do).** HamJEPA uses an *encoder-side* non-degeneracy bridge that avoids isotropic Gaussianity. It is useful to separate (i) scale control, (ii) rank/volume control, and (iii) spike control.

**Lemma A.9** (Scale budgets do not prevent rank collapse). *Fix  $c > 0$  and consider PSD matrices  $\Sigma \succeq 0$  with  $\text{tr}(\Sigma) = c$ . There exist such  $\Sigma$  with rank 1 (hence complete collapse except for one direction), e.g.  $\Sigma = \text{diag}(c, 0, \dots, 0)$ .*

*Proof.* See Appendix B.2.9. □

**Lemma A.10** (Log-det alone does not prevent “one-spike” spectra). *Fix  $k \geq 2$  and  $\tau \in \mathbb{R}$ . There exist positive definite  $\Sigma \in \mathbb{R}^{k \times k}$  with  $\frac{1}{k} \log \det(\Sigma) = \tau$  but with  $\text{PR}(\Sigma)$  arbitrarily close to 1 (spike regime).*

*Proof.* Appendix B.2.10. □

**Lemma A.11** (Participation ratio alone does not fix scale). *For any PSD  $\Sigma \succeq 0$  and any scalar  $a > 0$ ,  $\text{PR}(a\Sigma) = \text{PR}(\Sigma)$ . Thus a PR constraint alone does not prevent collapse by uniformly shrinking all eigenvalues.*

*Proof.* See Appendix B.2.11. □

**Lemma A.12** (Projected log-det detects full-space rank collapse). *Let  $Q \in \mathbb{R}^{d_0}$  be a zero-mean random vector with covariance  $\Sigma_Q \succeq 0$  and let  $R \in \mathbb{R}^{d_0 \times k}$  have full column rank  $k$  (e.g., orthonormal columns as in Sec. 4.3). Define the population projected covariance*

$$\Sigma_{Y,0} := R^\top \Sigma_Q R \in \mathbb{R}^{k \times k}.$$

*Then*

$$\text{rank}(\Sigma_{Y,0}) \leq \text{rank}(\Sigma_Q).$$

*In particular, if  $\text{rank}(\Sigma_Q) < k$  then  $\Sigma_{Y,0}$  is singular and therefore  $\det(\Sigma_{Y,0}) = 0$  and  $\log \det(\Sigma_{Y,0}) = -\infty$ .*

*Moreover, if one uses the ridge-regularized version from (34),*

$$\Sigma_Y := \Sigma_{Y,0} + \varepsilon I_k, \quad \varepsilon > 0,$$

*and if  $r := \text{rank}(\Sigma_{Y,0})$ , then  $\Sigma_Y$  has exactly  $k - r$  eigenvalues equal to  $\varepsilon$  and hence*

$$\log \det(\Sigma_Y) = (k - r) \log \varepsilon + \sum_{i=1}^r \log(\lambda_i + \varepsilon),$$

*where  $\lambda_1, \dots, \lambda_r > 0$  are the nonzero eigenvalues of  $\Sigma_{Y,0}$ .*

*Proof.* See Appendix B.2.12. □

**Projected log-det floor.** Recall the projected covariance  $\Sigma_Y$  from (34). The following proposition quantifies how a log-det floor plus a trace/scale control lower-bounds the smallest eigenvalue.

**Proposition A.13** (Projected log-det floor prevents rank collapse). *Let  $\Sigma_Y \in \mathbb{R}^{k \times k}$  be SPD with eigenvalues  $\lambda_1 \geq \dots \geq \lambda_k > 0$ . Suppose  $\log \det(\Sigma_Y) \geq k\tau$  and  $\text{tr}(\Sigma_Y) \leq m$  for some  $m > 0$ . Then*

$$\lambda_{\min}(\Sigma_Y) \geq \exp(k\tau) \frac{(k-1)^{k-1}}{m^{k-1}}. \quad (43)$$

*In particular, the representation cannot collapse onto a subspace of dimension  $< k$  in the projected sense.*

*Proof.* See Appendix B.2.13. □

**Joint spectral non-degeneracy (budget + log-det + PR).** The next theorem formalizes the “LogDet + PR + budget” bridge: it rules out both needle collapse and the one-spike “L-shaped” failure mode.

**Theorem A.14** (Spectral non-degeneracy via joint constraints). *Let  $\Sigma \in \mathbb{R}^{k \times k}$  be SPD with eigenvalues  $\lambda_1 \geq \dots \geq \lambda_k > 0$ . Assume the three constraints*

$$\text{tr}(\Sigma) = c, \quad \text{PR}(\Sigma) \geq r_0, \quad \frac{1}{k} \log \det(\Sigma) \geq \tau, \quad (44)$$

*for some  $c > 0$ ,  $r_0 \in (1, k]$ , and  $\tau \in \mathbb{R}$ . Then*

$$\lambda_{\max}(\Sigma) \leq \frac{c}{\sqrt{r_0}}; \quad \lambda_{\min}(\Sigma) \geq \exp(k\tau) \left( \frac{\sqrt{r_0}}{c} \right)^{k-1}. \quad (45)$$

*Consequently,  $\Sigma$  cannot realize the spike regime  $\lambda_1 \gg \lambda_2, \dots, \lambda_k$  and cannot approach rank collapse  $\lambda_{\min} \rightarrow 0$  under the stated floors.*

*Proof.* See Appendix B.2.14. □

**Corollary A.15** (Bounded conditioning under joint non-degeneracy constraints). *Under the assumptions of Theorem A.14, the condition number satisfies*

$$\kappa(\Sigma) := \frac{\lambda_{\max}(\Sigma)}{\lambda_{\min}(\Sigma)} \leq \exp(-k\tau) \left( \frac{c}{\sqrt{r_0}} \right)^k.$$

*Proof.* See Immediate by dividing the eigenvalue bounds in Theorem A.14. □

**Why symplecticity is still meaningful despite encoder regularizers.** Symplecticity constrains the predictor map, while the budget/volume/PR constraints constrain the encoder outputs. The next proposition states the correct conditional claim: if the encoder occupies nontrivial volume locally, then the symplectic predictor cannot destroy it.

**Proposition A.16** (Symplectic predictors cannot induce collapse). *Fix  $\phi$  and consider the predictor map  $\Phi_\phi^{(K)}$  from (28). If the encoder outputs occupy a set  $\mathcal{U} \subset \mathbb{R}^{2d_0}$  with positive Lebesgue volume, then  $\Phi_\phi^{(K)}(\mathcal{U})$  has the same volume as  $\mathcal{U}$ . In particular,  $\Phi_\phi^{(K)}$  cannot map a positive-volume set to a set of zero volume; any global representational collapse must arise from  $E_\theta$ , not from the symplectic predictor.*

*Proof.* See Appendix B.2.15. □

**Takeaway.** Theorems A.2 and A.4 ensure the predictor map is symplectic and volume-preserving (hence non-contracting in a precise geometric sense), with exact time reversibility (Corollary A.5) and reciprocal singular-value pairing (Lemma A.7). Since symplecticity alone does not prevent encoder collapse, HamJEPa uses a fixed-units scale budget plus projected log-det and PR floors; Theorem A.14 formalizes why the *combination* rules out both rank collapse and one-spike pathologies without enforcing isotropic Gaussian marginals.

## B Mathematical Proofs

### B.1 Proofs for Section 3

#### B.1.1 Proof of Lemma 3.1

Let  $\Sigma \succeq 0$  and  $H \succ 0$ . For  $w \in \mathcal{W}_H$ , define  $u := H^{-1/2}w$ . Then

$$w^\top H^{-1}w = \|H^{-1/2}w\|_2^2 = \|u\|_2^2 \leq 1,$$

so  $\mathcal{W}_H = \{H^{1/2}u : \|u\|_2 \leq 1\}$ . Substituting  $w = H^{1/2}u$  into the objective yields

$$w^\top \Sigma w = u^\top (H^{1/2} \Sigma H^{1/2}) u.$$

Therefore

$$V(\Sigma) = \sup_{\|u\|_2 \leq 1} u^\top (H^{1/2} \Sigma H^{1/2}) u = \lambda_{\max}(H^{1/2} \Sigma H^{1/2}),$$

where the last equality is the Rayleigh quotient characterization of the top eigenvalue. If  $u_{\max}$  is a unit top eigenvector of  $H^{1/2} \Sigma H^{1/2}$ , then the corresponding  $w_{\max} := H^{1/2}u_{\max}$  satisfies  $w_{\max}^\top H^{-1}w_{\max} = 1$  and attains the supremum.

#### B.1.2 Proof of Theorem 3.2

Let  $\Sigma \succeq 0$  and define

$$A := H^{1/2} \Sigma H^{1/2} \succeq 0.$$

Then  $\text{tr}(H\Sigma) = \text{tr}(A)$ , so the constraint  $\text{tr}(H\Sigma) = c$  becomes  $\text{tr}(A) = c$ . By Lemma 3.1, the objective is  $V(\Sigma) = \lambda_{\max}(A)$ . Thus (8) is equivalent to

$$\min_{A \succeq 0: \text{tr}(A)=c} \lambda_{\max}(A).$$

Let the eigenvalues of  $A$  be  $\lambda_1 \geq \dots \geq \lambda_d \geq 0$ . Then  $\sum_{i=1}^d \lambda_i = c$ , hence  $\lambda_1 \geq c/d$ . Therefore, for every feasible  $A$ ,

$$\lambda_{\max}(A) \geq \frac{c}{d}.$$

Equality  $\lambda_{\max}(A) = c/d$  holds if and only if  $\lambda_1 = \dots = \lambda_d = c/d$ , i.e.,  $A = (c/d)I$ , which is unique. Mapping back,

$$\Sigma^* = H^{-1/2} A H^{-1/2} = \frac{c}{d} H^{-1},$$

and the optimum value is  $c/d$ .

### B.1.3 Proof of Theorem 3.3

Let  $Z$  have a density,  $\mathbb{E}[Z] = 0$ , and satisfy  $\mathbb{E}[Z^\top H Z] = c$ . Define the invertible linear change of variables

$$Y := H^{1/2} Z.$$

Then  $\mathbb{E}[Y] = 0$  and

$$\mathbb{E}\|Y\|_2^2 = \mathbb{E}[Z^\top H Z] = c.$$

By the change-of-variables formula for differential entropy,

$$h(Z) = h(Y) + \log |\det(H^{-1/2})| = h(Y) - \frac{1}{2} \log \det(H).$$

Hence maximizing  $h(Z)$  under (11) is equivalent to maximizing  $h(Y)$  under  $\mathbb{E}\|Y\|_2^2 = c$ .

Let  $\Sigma_Y := \text{Cov}(Y) \succeq 0$ . A standard entropy bound states that for any random vector with covariance  $\Sigma_Y$ ,

$$h(Y) \leq \frac{1}{2} \log \left( (2\pi e)^d \det(\Sigma_Y) \right),$$

with equality if and only if  $Y$  is Gaussian with covariance  $\Sigma_Y$ .

Next, the constraint  $\mathbb{E}\|Y\|_2^2 = c$  implies  $\text{tr}(\Sigma_Y) = c$  (since  $\mathbb{E}[Y] = 0$ ). For any PSD matrix with eigenvalues  $\nu_1, \dots, \nu_d \geq 0$  and fixed sum  $\sum_i \nu_i = c$ , the arithmetic–geometric mean inequality gives

$$\det(\Sigma_Y) = \prod_{i=1}^d \nu_i \leq \left( \frac{1}{d} \sum_{i=1}^d \nu_i \right)^d = \left( \frac{c}{d} \right)^d,$$

with equality if and only if  $\nu_1 = \dots = \nu_d = c/d$ , i.e.,  $\Sigma_Y = (c/d)I$ .

Combining the two inequalities yields

$$h(Y) \leq \frac{1}{2} \log \left( (2\pi e)^d (c/d)^d \right),$$

with equality if and only if  $Y \sim \mathcal{N}(0, (c/d)I)$ . Therefore the unique maximizer is  $Y \sim \mathcal{N}(0, (c/d)I)$ , and hence

$$Z = H^{-1/2} Y \sim \mathcal{N}\left(0, \frac{c}{d} H^{-1}\right),$$

as claimed.

### B.1.4 Proof of Theorem 3.4

Under Euclidean isotropy  $\Sigma = \sigma^2 I$ , the budget  $\text{tr}(H\Sigma) = c$  forces

$$\sigma^2 \text{tr}(H) = c \quad \Rightarrow \quad \sigma^2 = \frac{c}{\text{tr}(H)},$$

so  $\Sigma_{\text{iso}} = \frac{c}{\text{tr}(H)} I$ .

Using Lemma 3.1,

$$V(\Sigma_{\text{iso}}) = \lambda_{\max}(H^{1/2} \Sigma_{\text{iso}} H^{1/2}) = \lambda_{\max}\left(\frac{c}{\text{tr}(H)} H\right) = \frac{c}{\text{tr}(H)} \lambda_{\max}(H),$$

which is (14). From Theorem 3.2,  $V(\Sigma^*) = c/d$ , so the ratio is

$$\frac{V(\Sigma_{\text{iso}})}{V(\Sigma^*)} = \frac{\frac{c}{\text{tr}(H)} \lambda_{\max}(H)}{c/d} = \frac{d \lambda_{\max}(H)}{\text{tr}(H)} = \rho(H).$$

Since  $\lambda_{\max}(H) \geq \text{tr}(H)/d$  for any SPD  $H$ , we have  $\rho(H) \geq 1$ . Also  $\lambda_{\max}(H) \leq \text{tr}(H)$  implies  $\rho(H) \leq d$ . Finally,  $\rho(H) = 1$  holds if and only if  $\lambda_{\max}(H) = \text{tr}(H)/d$ , which occurs if and only if all eigenvalues of  $H$  are equal, i.e.  $H \propto I$ .

### B.1.5 Proof of Proposition 3.5

Let  $\mu := \mathbb{E}[Z]$  so that  $\Sigma = \mathbb{E}[(Z - \mu)(Z - \mu)^\top]$ . Define  $Z' := H^{1/2}Z$  and note  $\mathbb{E}[Z'] = H^{1/2}\mu$ . Then

$$\begin{aligned}\text{Cov}(Z') &= \mathbb{E}[(Z' - \mathbb{E}[Z'])(Z' - \mathbb{E}[Z'])^\top] \\ &= \mathbb{E}[H^{1/2}(Z - \mu)(Z - \mu)^\top(H^{1/2})^\top] \\ &= H^{1/2} \mathbb{E}[(Z - \mu)(Z - \mu)^\top] (H^{1/2})^\top \\ &= H^{1/2} \Sigma H^{1/2},\end{aligned}$$

where we used that  $H^{1/2}$  is symmetric for SPD  $H$ .

For the equivalence: if  $\Sigma = \alpha H^{-1}$  then

$$\text{Cov}(Z') = H^{1/2}(\alpha H^{-1})H^{1/2} = \alpha I.$$

Conversely, if  $\text{Cov}(Z') = \alpha I$ , multiply left and right by  $H^{-1/2}$  to obtain

$$\Sigma = H^{-1/2}(\alpha I)H^{-1/2} = \alpha H^{-1}.$$

□

### B.1.6 Proof of Proposition 3.6

By definition,

$$\mathcal{H}_H(q, p) = \frac{1}{2}q^\top Hq + \frac{1}{2}\|p\|_2^2,$$

so

$$\pi_H(q, p) = \frac{1}{Z_H} \exp\left(-\frac{d}{2c}q^\top Hq\right) \exp\left(-\frac{d}{2c}\|p\|_2^2\right).$$

Hence the density factorizes into a  $q$ -term and a  $p$ -term, so  $q$  and  $p$  are independent.

The partition function also factorizes:

$$Z_H = \left(\int_{\mathbb{R}^d} \exp\left(-\frac{d}{2c}q^\top Hq\right) dq\right) \left(\int_{\mathbb{R}^d} \exp\left(-\frac{d}{2c}\|p\|_2^2\right) dp\right).$$

Using the standard Gaussian integral

$$\int_{\mathbb{R}^d} \exp\left(-\frac{1}{2}x^\top Ax\right) dx = (2\pi)^{d/2} \det(A)^{-1/2} \quad (A \succ 0),$$

with  $A = (d/c)H$  for the  $q$ -integral and  $A = (d/c)I$  for the  $p$ -integral, we obtain

$$Z_H = \left(2\pi \frac{c}{d}\right)^d \det(H)^{-1/2}.$$

Therefore

$$\pi_H(q, p) = \underbrace{\left(2\pi \frac{c}{d}\right)^{-d/2} \det(H)^{1/2} \exp\left(-\frac{d}{2c}q^\top Hq\right)}_{q\text{-marginal}} \cdot \underbrace{\left(2\pi \frac{c}{d}\right)^{-d/2} \exp\left(-\frac{d}{2c}\|p\|_2^2\right)}_{p\text{-marginal}}.$$

Thus  $q$  is Gaussian with precision matrix  $(d/c)H$ , hence covariance  $(c/d)H^{-1}$ , and  $p$  is Gaussian with precision  $(d/c)I$ , hence covariance  $(c/d)I$ :

$$q \sim \mathcal{N}\left(0, \frac{c}{d}H^{-1}\right), \quad p \sim \mathcal{N}\left(0, \frac{c}{d}I\right).$$

Next,

$$\mathbb{E}_{\pi_H}[q^\top Hq] = \text{tr}(H \text{Cov}(q)) = \text{tr}\left(H \frac{c}{d}H^{-1}\right) = \frac{c}{d} \text{tr}(I) = c.$$

Similarly,

$$\mathbb{E}_{\pi_H}[\|p\|_2^2] = \text{tr}(\text{Cov}(p)) = \text{tr}\left(\frac{c}{d}I\right) = c.$$

Hence

$$\mathbb{E}_{\pi_H}[\mathcal{H}_H(q, p)] = \frac{1}{2} \mathbb{E}_{\pi_H}[q^\top H q] + \frac{1}{2} \mathbb{E}_{\pi_H}[\|p\|_2^2] = \frac{1}{2}c + \frac{1}{2}c = c.$$

Finally, the  $q$ -marginal is exactly the Gaussian

$$\mathcal{N}\left(0, \frac{c}{d}H^{-1}\right),$$

which is the minimax-optimal covariance from Theorem 3.2 and the maximum-entropy law from Theorem 3.3.  $\square$

### B.1.7 Proof of Proposition 3.7

Let  $\Sigma \succ 0$  be arbitrary and define

$$H := \frac{c}{d}\Sigma^{-1}.$$

Since  $\Sigma^{-1} \succ 0$ , we have  $H \succ 0$ . Then

$$\Sigma^*(H) = \frac{c}{d}H^{-1} = \frac{c}{d} \left(\frac{c}{d}\Sigma^{-1}\right)^{-1} = \frac{c}{d} \cdot \frac{d}{c}\Sigma = \Sigma.$$

Thus every  $\Sigma \succ 0$  arises as  $\Sigma^*(H)$  for some  $H \succ 0$ , so the family  $\{\Sigma^*(H) : H \succ 0\}$  is exactly the SPD cone.  $\square$

### B.1.8 Proof of Theorem 3.8

First note that  $\Sigma_M(H)$  is feasible for the  $H$ -budget:

$$\text{tr}(H\Sigma_M(H)) = \text{tr}\left(H \frac{c}{\text{tr}(HM)}M\right) = c.$$

By the spectral form of the worst-case task variance,

$$V_H(\Sigma) = \lambda_{\max}\left(H^{1/2}\Sigma H^{1/2}\right).$$

Therefore

$$V_H(\Sigma_M(H)) = \lambda_{\max}\left(H^{1/2} \frac{c}{\text{tr}(HM)} M H^{1/2}\right) = \frac{c}{\text{tr}(HM)} \lambda_{\max}\left(H^{1/2} M H^{1/2}\right).$$

For the oracle covariance

$$\Sigma^*(H) = \frac{c}{d}H^{-1},$$

we have

$$H^{1/2}\Sigma^*(H)H^{1/2} = \frac{c}{d}I,$$

so

$$V_H(\Sigma^*(H)) = \frac{c}{d}.$$

Dividing the two expressions gives

$$\frac{V_H(\Sigma_M(H))}{V_H(\Sigma^*(H))} = \frac{\frac{c}{\text{tr}(HM)} \lambda_{\max}(H^{1/2} M H^{1/2})}{c/d} = \frac{d \lambda_{\max}(H^{1/2} M H^{1/2})}{\text{tr}(HM)}.$$

Since

$$\text{tr}(HM) = \text{tr}\left(H^{1/2} M H^{1/2}\right),$$

writing

$$A := H^{1/2} M H^{1/2} \succ 0$$

gives

$$\frac{V_H(\Sigma_M(H))}{V_H(\Sigma^*(H))} = \frac{d \lambda_{\max}(A)}{\text{tr}(A)}.$$

For any  $A \succ 0$ ,

$$\lambda_{\max}(A) \leq \text{tr}(A) \leq d \lambda_{\max}(A),$$

and hence

$$1 \leq \frac{d \lambda_{\max}(A)}{\text{tr}(A)} \leq d.$$

The ratio equals 1 if and only if

$$\text{tr}(A) = d \lambda_{\max}(A),$$

which holds if and only if all eigenvalues of  $A$  are equal, i.e.

$$A = \alpha I$$

for some  $\alpha > 0$ . Since  $A = H^{1/2} M H^{1/2}$ , this is equivalent to

$$H^{1/2} M H^{1/2} = \alpha I,$$

or, multiplying on the left and right by  $H^{-1/2}$ ,

$$M = \alpha H^{-1}.$$

Thus the regret is 1 if and only if  $M \propto H^{-1}$ .

It remains to show that, for every fixed  $M \succ 0$ , the supremum over  $H \succ 0$  is  $d$ . The upper bound  $d$  was just shown. To see that it is sharp, fix  $\delta > 0$  and define

$$A_\delta := \text{diag}(1, \delta, \dots, \delta) \succ 0.$$

We claim there exists  $H_\delta \succ 0$  such that

$$H_\delta^{1/2} M H_\delta^{1/2} = A_\delta.$$

Indeed, let

$$B_\delta := M^{-1/2} \left( M^{1/2} A_\delta M^{1/2} \right)^{1/2} M^{-1/2} \succ 0$$

and set

$$H_\delta := B_\delta^2.$$

Then  $H_\delta^{1/2} = B_\delta$  and

$$H_\delta^{1/2} M H_\delta^{1/2} = B_\delta M B_\delta = A_\delta.$$

For this choice,

$$\frac{V_{H_\delta}(\Sigma_M(H_\delta))}{V_{H_\delta}(\Sigma^*(H_\delta))} = \frac{d \lambda_{\max}(A_\delta)}{\text{tr}(A_\delta)} = \frac{d}{1 + (d-1)\delta}.$$

Letting  $\delta \downarrow 0$  gives

$$\sup_{H \succ 0} \frac{V_H(\Sigma_M(H))}{V_H(\Sigma^*(H))} = d.$$

For  $d = 1$ , the same conclusion is immediate since the ratio is identically  $1 = d$ . Thus no geometry-independent fixed covariance shape  $M$  is canonical for all structured geometries.

### B.1.9 Proof of Proposition 3.9

Because  $(Z_a, Z_b)$  is jointly Gaussian, any affine transformation of  $(Z_a, Z_b)$  is also Gaussian. Define the residual

$$R := Z_b - C \Sigma^{-1} Z_a.$$

Then

$$\text{Cov}(R, Z_a) = \text{Cov}(Z_b, Z_a) - C \Sigma^{-1} \text{Cov}(Z_a, Z_a) = C - C \Sigma^{-1} \Sigma = 0.$$

Since  $(R, Z_a)$  is jointly Gaussian and uncorrelated,  $R$  and  $Z_a$  are independent. Also, because the variables are centered,

$$\mathbb{E}[R] = 0.$$

Therefore

$$\mathbb{E}[Z_b | Z_a] = \mathbb{E}[C \Sigma^{-1} Z_a + R | Z_a] = C \Sigma^{-1} Z_a + \mathbb{E}[R | Z_a] = C \Sigma^{-1} Z_a.$$

It remains to show that the same marginal covariance  $\Sigma$  admits many different predictive maps. For any  $t \in (-1, 1)$ , consider the block covariance

$$\Gamma_t := \begin{pmatrix} \Sigma & t\Sigma \\ t\Sigma & \Sigma \end{pmatrix}.$$

For any  $u, v \in \mathbb{R}^d$ ,

$$\begin{pmatrix} u \\ v \end{pmatrix}^\top \Gamma_t \begin{pmatrix} u \\ v \end{pmatrix} = u^\top \Sigma u + 2t u^\top \Sigma v + v^\top \Sigma v.$$

Equivalently,

$$u^\top \Sigma u + 2t u^\top \Sigma v + v^\top \Sigma v = \frac{1+t}{2} (u+v)^\top \Sigma (u+v) + \frac{1-t}{2} (u-v)^\top \Sigma (u-v).$$

Since  $\Sigma \succ 0$  and  $t \in (-1, 1)$ , this quadratic form is strictly positive for every nonzero  $(u, v)$ . Hence  $\Gamma_t \succ 0$ , so it defines a valid centered joint Gaussian law with both marginals equal to  $\Sigma$  and cross-covariance

$$C_t = t\Sigma.$$

For this joint law, the Bayes predictor is

$$\mathbb{E}[Z_b | Z_a] = C_t \Sigma^{-1} Z_a = t Z_a.$$

As  $t$  varies over  $(-1, 1)$ , the marginal covariance of both views remains exactly  $\Sigma$ , but the predictive map varies continuously from nearly  $-Z_a$  to nearly  $Z_a$ . Thus even an oracle marginal covariance does not identify the view-to-view coupling. Marginal matching alone therefore cannot determine the JEPA predictive problem.

## B.2 Proofs for Section 4.4

### B.2.1 Proof of Lemma A.1

By definition,  $\mathbf{Z}' = \mathbf{Z}H^{1/2}$ , so its  $i$ th row is

$$(\mathbf{Z}')_{i,:} = (\mathbf{Z}_{i,:})H^{1/2} = z_i^\top H^{1/2}.$$

Taking transpose gives

$$(\mathbf{Z}')_{i,:}^\top = (z_i^\top H^{1/2})^\top = (H^{1/2})^\top z_i = H^{1/2} z_i,$$

where we used symmetry of  $H^{1/2}$  (valid for SPD  $H$ ).

### B.2.2 Proof of Theorem A.2

Fix  $s_0 \in \mathbb{R}^{2d_0}$  and let  $s(t) = \Phi_{\phi,t}(s_0)$  solve  $\dot{s} = J\nabla\mathcal{H}_\phi(s)$ . Let  $A(t) := D\Phi_{\phi,t}(s_0) \in \mathbb{R}^{2d_0 \times 2d_0}$  denote the Jacobian of the flow with respect to the initial condition. Differentiating the ODE with respect to  $s_0$  yields the variational equation

$$\dot{A}(t) = J\nabla^2\mathcal{H}_\phi(s(t))A(t), \quad A(0) = I. \quad (46)$$

Define  $M(t) := A(t)^\top JA(t)$ . Using (46) and the facts  $J^\top = -J$  and  $\nabla^2\mathcal{H}_\phi$  is symmetric, we compute

$$\dot{M}(t) = \dot{A}(t)^\top JA(t) + A(t)^\top J\dot{A}(t) = A(t)^\top \nabla^2\mathcal{H}_\phi(s(t))^\top J^\top JA(t) + A(t)^\top JJ\nabla^2\mathcal{H}_\phi(s(t))A(t).$$

Since  $\nabla^2\mathcal{H}_\phi(s(t))^\top = \nabla^2\mathcal{H}_\phi(s(t))$  and  $J^\top = -J$  and  $JJ = -I$ , this becomes

$$\dot{M}(t) = A(t)^\top \nabla^2\mathcal{H}_\phi(s(t)) (-J)JA(t) + A(t)^\top (-I)\nabla^2\mathcal{H}_\phi(s(t))A(t) = A(t)^\top \nabla^2\mathcal{H}_\phi(s(t))A(t) - A(t)^\top \nabla^2\mathcal{H}_\phi(s(t))A(t) = 0.$$

Thus  $M(t)$  is constant in  $t$ . At  $t = 0$ ,  $A(0) = I$  so  $M(0) = J$ , hence  $M(t) = J$  for all  $t$ , proving (40).

For the determinant claim, take determinants of  $A(t)^\top JA(t) = J$ :

$$\det(A(t))^2 \det(J) = \det(J) \quad \Rightarrow \quad \det(A(t))^2 = 1.$$

Since  $A(0) = I$  has  $\det(A(0)) = 1$  and  $\det(A(t))$  varies continuously with  $t$ , we must have  $\det(A(t)) = 1$  for all  $t$ .

Finally, volume preservation follows from  $\det(D\Phi_{\phi,t}(s)) \equiv 1$  by the change-of-variables theorem: for any measurable set  $U$ ,

$$\text{Vol}(\Phi_{\phi,t}(U)) = \int_U |\det(D\Phi_{\phi,t}(s))| ds = \int_U 1 ds = \text{Vol}(U).$$

### B.2.3 Proof of Corollary A.3

Let  $Y = F(X)$  with  $F$  a  $C^1$  diffeomorphism. The change-of-variables formula gives  $p_Y(y) = p_X(x) |\det(DF(x))|^{-1}$  with  $x = F^{-1}(y)$ . Then

$$h(Y) = - \int p_Y(y) \log p_Y(y) dy = - \int p_X(x) \log (p_X(x) |\det(DF(x))|^{-1}) dx = h(X) + \mathbb{E}[\log |\det(DF(X))|].$$

If  $|\det(DF(\cdot))| \equiv 1$ , the second term is zero, so  $h(Y) = h(X)$ .

### B.2.4 Proof of Theorem A.4

Write the leapfrog step as a composition of two “kicks” and one “drift”. Define for  $h \in \mathbb{R}$ :

$$K_h(q, p) := (q, p - h\nabla V_\phi(q)), \quad D_h(q, p) := (q + hp, p),$$

where the drift uses  $\nabla T(p) = p$  for  $T(p) = \frac{1}{2}\|p\|^2$ . Then the one-step leapfrog map satisfies

$$\Psi_{\phi, \Delta t} = K_{\Delta t/2} \circ D_{\Delta t} \circ K_{\Delta t/2}.$$

We show that both  $K_h$  and  $D_h$  are symplectic. Their Jacobians have block forms

$$DK_h(q, p) = \begin{pmatrix} I & 0 \\ -h\nabla^2 V_\phi(q) & I \end{pmatrix} = \begin{pmatrix} I & 0 \\ B & I \end{pmatrix}, \quad B^\top = B, \quad DD_h(q, p) = \begin{pmatrix} I & hI \\ 0 & I \end{pmatrix} = \begin{pmatrix} I & C \\ 0 & I \end{pmatrix}, \quad C^\top = C.$$

A direct calculation shows that any matrix of the form  $\begin{pmatrix} I & 0 \\ B & I \end{pmatrix}$  with  $B$  symmetric satisfies  $A^\top J A = J$ , and similarly for  $\begin{pmatrix} I & C \\ 0 & I \end{pmatrix}$  with  $C$  symmetric. Therefore  $DK_h$  and  $DD_h$  are symplectic matrices at every point, so  $K_h$  and  $D_h$  are symplectic maps.

The composition of symplectic maps is symplectic, hence  $\Psi_{\phi, \Delta t}$  is symplectic, and iterating yields symplecticity of  $\Phi_\phi^{(K)} = \Psi_{\phi, \Delta t}^K$ . The determinant claim follows as in the proof of Theorem A.2.

### B.2.5 Proof of Corollary A.5

Using the decomposition  $\Psi_{\Delta t} = K_{\Delta t/2} \circ D_{\Delta t} \circ K_{\Delta t/2}$ , we have  $K_h^{-1} = K_{-h}$  and  $D_h^{-1} = D_{-h}$  by inspection. Hence

$$\Psi_{\Delta t}^{-1} = K_{\Delta t/2}^{-1} \circ D_{\Delta t}^{-1} \circ K_{\Delta t/2}^{-1} = K_{-\Delta t/2} \circ D_{-\Delta t} \circ K_{-\Delta t/2} = \Psi_{-\Delta t}.$$

Taking  $K$ -fold compositions gives  $(\Psi_{\Delta t}^K)^{-1} = \Psi_{-\Delta t}^K$ .

### B.2.6 Proof of Proposition A.6

Write the phase-space state as  $s = (q, p) \in \mathbb{R}^{2d_0}$  and define the two vector fields

$$f(s) := \begin{pmatrix} p \\ -\nabla V(q) \end{pmatrix}, \quad f_\phi(s) := \begin{pmatrix} p \\ -\nabla V_\phi(q) \end{pmatrix}.$$

Let  $\Phi_t^V$  denote the flow of  $\dot{s} = f(s)$  and  $\Phi_t^{V_\phi}$  the flow of  $\dot{s} = f_\phi(s)$ .

Throughout, work on the compact set  $\Omega = \Omega_q \times \Omega_p$  from the proposition statement. Since  $\nabla V$  and  $\nabla V_\phi$  are Lipschitz on  $\Omega_q$  and  $\Omega_p$  is compact, both  $f$  and  $f_\phi$  are Lipschitz on  $\Omega$ ; let  $L$  be any Lipschitz constant of  $f_\phi$  on  $\Omega$ :

$$\|f_\phi(x) - f_\phi(y)\|_2 \leq L\|x - y\|_2, \quad \forall x, y \in \Omega.$$

Define the uniform force mismatch on  $\Omega_q$ :

$$\delta := \sup_{q \in \Omega_q} \|\nabla V_\phi(q) - \nabla V(q)\|_2.$$

**Step 1: Continuous dependence of flows on the force field.** Fix  $s_0 \in K$  and let  $s(t) := \Phi_t^V(s_0)$  and  $\tilde{s}(t) := \Phi_t^{V_\phi}(s_0)$ . By assumption, both trajectories remain in  $\Omega$  for  $t \in [0, T]$ . Let  $\Delta(t) := \tilde{s}(t) - s(t)$ . Then

$$\begin{aligned}\dot{\Delta}(t) &= f_\phi(\tilde{s}(t)) - f(s(t)) \\ &= (f_\phi(\tilde{s}(t)) - f_\phi(s(t))) + (f_\phi(s(t)) - f(s(t))).\end{aligned}$$

Taking norms and using Lipschitzness of  $f_\phi$  on  $\Omega$  plus the definition of  $\delta$  gives

$$\|\dot{\Delta}(t)\|_2 \leq L\|\Delta(t)\|_2 + \delta.$$

Since  $\Delta(0) = 0$ , Grönwall's inequality yields, for all  $t \in [0, T]$ ,

$$\|\Delta(t)\|_2 \leq \begin{cases} \frac{\delta}{L}(e^{Lt} - 1), & L > 0, \\ \delta t, & L = 0. \end{cases}$$

In particular, at  $t = T$  we obtain a uniform (over  $s_0 \in K$ ) modeling-error bound

$$\sup_{s_0 \in K} \|\Phi_T^{V_\phi}(s_0) - \Phi_T^V(s_0)\|_2 \leq C_1 \delta, \quad C_1 := \begin{cases} \frac{e^{LT} - 1}{L}, & L > 0, \\ T, & L = 0. \end{cases}$$

**Step 2: Leapfrog global error is  $O(\Delta t^2)$ .** Fix  $\phi$  and consider the ODE  $\dot{s} = f_\phi(s)$ . Let  $\Psi_{\phi, h}$  denote one leapfrog step with step size  $h$  (Eq. (29)), and define the numerical iterates

$$s_{n+1} := \Psi_{\phi, h}(s_n), \quad s_0 \in K, \quad t_n := nh,$$

so that  $s_K = (\Psi_{\phi, h})^K(s_0) = \Phi_\phi^{(K)}(s_0)$  with  $Kh = T$ .

(2a) *Local truncation error bound.* Because  $V_\phi \in C^3$  on a neighborhood of  $\Omega_q$ , the vector fields

$$A(q, p) := \begin{pmatrix} p \\ 0 \end{pmatrix}, \quad B(q, p) := \begin{pmatrix} 0 \\ -\nabla V_\phi(q) \end{pmatrix}$$

are  $C^2$  on  $\Omega$ , and their exact flows are

$$\exp(hA) : (q, p) \mapsto (q + hp, p), \quad \exp(hB) : (q, p) \mapsto (q, p - h\nabla V_\phi(q)).$$

The leapfrog step is exactly the Strang splitting:

$$\Psi_{\phi, h} = \exp\left(\frac{h}{2}B\right) \exp(hA) \exp\left(\frac{h}{2}B\right).$$

Standard Strang splitting theory (derivable via the BCH expansion for the Lie operators  $L_A, L_B$ ) implies that the local truncation error is third order: there exists a constant  $C_{\text{loc}} = C_{\text{loc}}(\Omega, V_\phi)$  such that

$$\sup_{x \in \Omega} \|\Psi_{\phi, h}(x) - \Phi_h^{V_\phi}(x)\|_2 \leq C_{\text{loc}} h^3 \quad \text{for all sufficiently small } h.$$

(Concretely, the BCH expansion gives  $\exp(\frac{h}{2}L_B) \exp(hL_A) \exp(\frac{h}{2}L_B) = \exp(h(L_A + L_B)) + O(h^3)$ ) as operators on smooth test functions, and boundedness of the commutators on  $\Omega$  yields the uniform  $C_{\text{loc}}$ .)

(2b) *Error recursion and discrete Grönwall.* Define the global error at step  $n$  by

$$e_n := s_n - \Phi_{t_n}^{V_\phi}(s_0).$$

Then

$$\begin{aligned}e_{n+1} &= \Psi_{\phi, h}(s_n) - \Phi_{t_{n+1}}^{V_\phi}(s_0) \\ &= \Psi_{\phi, h}(s_n) - \Phi_h^{V_\phi}(\Phi_{t_n}^{V_\phi}(s_0)).\end{aligned}$$

Add and subtract  $\Phi_h^{V_\phi}(s_n)$ :

$$e_{n+1} = \underbrace{(\Psi_{\phi, h}(s_n) - \Phi_h^{V_\phi}(s_n))}_{\text{local truncation}} + \underbrace{(\Phi_h^{V_\phi}(s_n) - \Phi_h^{V_\phi}(\Phi_{t_n}^{V_\phi}(s_0)))}_{\text{stability}}.$$

Taking norms, using the local error bound from (2a), and using Lipschitz stability of the flow  $\|\Phi_h^{V_\phi}(x) - \Phi_h^{V_\phi}(y)\|_2 \leq e^{Lh}\|x - y\|_2$  on  $\Omega$  yields

$$\|e_{n+1}\|_2 \leq C_{\text{loc}}h^3 + e^{Lh}\|e_n\|_2.$$

Iterating this recursion with  $e_0 = 0$  gives

$$\|e_K\|_2 \leq C_{\text{loc}}h^3 \sum_{j=0}^{K-1} e^{Lhj} = C_{\text{loc}}h^3 \cdot \begin{cases} \frac{e^{LK} - 1}{e^{Lh} - 1}, & L > 0, \\ K, & L = 0. \end{cases}$$

Since  $Kh = T$  and  $e^{Lh} - 1 \geq Lh$  for  $Lh \geq 0$ , we obtain

$$\|e_K\|_2 \leq \begin{cases} \frac{C_{\text{loc}}}{L}(e^{LT} - 1)h^2, & L > 0, \\ C_{\text{loc}}Th^2, & L = 0. \end{cases}$$

Taking the supremum over  $s_0 \in K$  (all iterates stay in  $\Omega$  by assumption), we conclude that there exists  $C_2 = C_2(T, \Omega, V_\phi)$  such that

$$\sup_{s_0 \in K} \|\Phi_\phi^{(K)}(s_0) - \Phi_T^{V_\phi}(s_0)\|_2 \leq C_2 h^2.$$

**Step 3: Combine modeling and integrator errors.** By the triangle inequality,

$$\|\Phi_\phi^{(K)}(s_0) - \Phi_T^V(s_0)\|_2 \leq \|\Phi_\phi^{(K)}(s_0) - \Phi_T^{V_\phi}(s_0)\|_2 + \|\Phi_T^{V_\phi}(s_0) - \Phi_T^V(s_0)\|_2.$$

Taking suprema over  $s_0 \in K$  and applying the bounds from Steps 1–2 yields

$$\sup_{s_0 \in K} \|\Phi_\phi^{(K)}(s_0) - \Phi_T^V(s_0)\|_2 \leq C_2 h^2 + C_1 \delta.$$

This is the claimed inequality with  $C := \max\{C_1, C_2\}$  (or  $C := C_1 + C_2$ ).

Finally, if the model class can make  $\delta$  arbitrarily small (uniform approximation of  $\nabla V$  on  $\Omega_q$ ), choose  $\phi$  so that  $C_1 \delta \leq \varepsilon/2$ , then choose  $h = \Delta t$  so that  $C_2 h^2 \leq \varepsilon/2$ , and conclude

$$\sup_{s_0 \in K} \|\Phi_\phi^{(K)}(s_0) - \Phi_T^V(s_0)\|_2 \leq \varepsilon.$$

□

### B.2.7 Proof of Lemma A.7

Let  $A$  be symplectic:  $A^\top J A = J$ . Using  $J^{-1} = -J$  and  $J^\top = -J$ , we obtain

$$A^{-1} = -J A^\top J.$$

Then

$$(A^\top A)^{-1} = A^{-1} A^{-T} = (-J A^\top J)(-J A J) = J^{-1} (A^\top A) J,$$

so  $(A^\top A)^{-1}$  is similar to  $A^\top A$  and thus has the same eigenvalues. Therefore the eigenvalues of  $A^\top A$  occur in reciprocal pairs  $(\mu, 1/\mu)$ , and the singular values  $\sigma = \sqrt{\mu}$  occur in reciprocal pairs  $(\sigma, 1/\sigma)$ .

### B.2.8 Proof sketch of Theorem A.8

This is a standard result from backward error analysis for symplectic integrators; we provide the BCH-based sketch specialized to leapfrog.

Let  $L_T$  and  $L_V$  denote the Lie derivatives (Poisson bracket operators) corresponding to the Hamiltonians  $T$  and  $V$ , acting on smooth observables. The exact time- $h$  flow of  $T$  (resp.  $V$ ) is  $\exp(hL_T)$  (resp.  $\exp(hL_V)$ ). The leapfrog step can be written operator-theoretically as the symmetric composition

$$\exp\left(\frac{h}{2}L_V\right) \exp(hL_T) \exp\left(\frac{h}{2}L_V\right).$$

By the Baker–Campbell–Hausdorff (BCH) formula, this equals

$$\exp\left(h(L_T + L_V) + h^3 C_3 + h^5 C_5 + \dots\right),$$

where  $C_3, C_5, \dots$  are nested commutators of  $L_T$  and  $L_V$ . For Hamiltonian systems, commutators of Hamiltonian vector fields correspond to Hamiltonian vector fields of Poisson brackets; equivalently, each  $C_{2j+1}$  is itself a Lie derivative  $L_{H_{2j}}$  for some scalar function  $H_{2j}$  built from iterated Poisson brackets of  $T$  and  $V$ . Thus the exponential above is the exact time- $h$  flow of a *modified Hamiltonian*

$$\tilde{\mathcal{H}}_{\Delta t} = \mathcal{H} + h^2 H_2 + h^4 H_4 + \dots$$

at the level of formal series. Truncating this series at order  $N$  yields a modified Hamiltonian  $\tilde{\mathcal{H}}_{\Delta t}^{[N]}$  whose flow matches one leapfrog step up to local error  $\mathcal{O}(h^{N+1})$ . Under analyticity, classical results show that the truncation can be chosen so that the resulting modified energy is nearly conserved over exponentially long times in  $1/h$ . (See, e.g., standard references on geometric numerical integration for full details.)

### B.2.9 Proof of Lemma A.9

Take  $\Sigma = \text{diag}(c, 0, \dots, 0)$ . Then  $\Sigma \succeq 0$ ,  $\text{tr}(\Sigma) = c$ , and  $\text{rank}(\Sigma) = 1$ .

### B.2.10 Proof of Lemma A.10

Fix  $k \geq 2$  and  $\tau$ . For  $\varepsilon > 0$ , define eigenvalues

$$\lambda_2 = \dots = \lambda_k = \varepsilon, \quad \lambda_1 = \exp(k\tau) \varepsilon^{-(k-1)}.$$

Then  $\prod_{i=1}^k \lambda_i = \exp(k\tau)$ , hence  $\frac{1}{k} \log \det(\Sigma) = \tau$ . But as  $\varepsilon \rightarrow 0$ ,  $\lambda_1 \rightarrow \infty$  and  $\lambda_2, \dots, \lambda_k \rightarrow 0$ . The participation ratio satisfies

$$\text{PR}(\Sigma) = \frac{(\sum_i \lambda_i)^2}{\sum_i \lambda_i^2} \rightarrow \frac{\lambda_1^2}{\lambda_1^2} = 1,$$

so  $\text{PR}(\Sigma)$  can be made arbitrarily close to 1 while maintaining the log-det constraint.

### B.2.11 Proof of Lemma A.11

Let  $\lambda_i$  be the eigenvalues of  $\Sigma$ . Then the eigenvalues of  $a\Sigma$  are  $a\lambda_i$ , so

$$\text{PR}(a\Sigma) = \frac{(\sum_i a\lambda_i)^2}{\sum_i (a\lambda_i)^2} = \frac{a^2(\sum_i \lambda_i)^2}{a^2 \sum_i \lambda_i^2} = \text{PR}(\Sigma).$$

### B.2.12 Proof of Lemma A.12

Let  $\Sigma_Q \succeq 0$  and  $R \in \mathbb{R}^{d_0 \times k}$  have full column rank. Write  $\Sigma_Q = A^\top A$  with  $A := \Sigma_Q^{1/2}$  (PSD square root). Then

$$\Sigma_{Y,0} = R^\top \Sigma_Q R = R^\top A^\top A R = (AR)^\top (AR).$$

Therefore  $\Sigma_{Y,0}$  is PSD and

$$\text{rank}(\Sigma_{Y,0}) = \text{rank}((AR)^\top (AR)) = \text{rank}(AR) \leq \text{rank}(A) = \text{rank}(\Sigma_Q).$$

If  $\text{rank}(\Sigma_Q) < k$ , then  $\text{rank}(\Sigma_{Y,0}) < k$ , so  $\Sigma_{Y,0}$  is singular. Hence  $\det(\Sigma_{Y,0}) = 0$  and  $\log \det(\Sigma_{Y,0}) = -\infty$ .

For the ridge statement, let  $r := \text{rank}(\Sigma_{Y,0})$  and let  $\lambda_1, \dots, \lambda_r > 0$  be its nonzero eigenvalues. Then  $\Sigma_{Y,0}$  has exactly  $k-r$  zero eigenvalues. Adding  $\varepsilon I_k$  shifts each eigenvalue by  $\varepsilon$ , so  $\Sigma_Y = \Sigma_{Y,0} + \varepsilon I_k$  has eigenvalues

$$\lambda_1 + \varepsilon, \dots, \lambda_r + \varepsilon, \underbrace{\varepsilon, \dots, \varepsilon}_{k-r \text{ times}}.$$

Thus

$$\log \det(\Sigma_Y) = \sum_{i=1}^r \log(\lambda_i + \varepsilon) + (k-r) \log \varepsilon,$$

which is exactly the claimed formula.  $\square$

### B.2.13 Proof of Proposition A.13

Let  $\lambda_1 \geq \dots \geq \lambda_k > 0$  be eigenvalues of  $\Sigma_Y$ . From  $\log \det(\Sigma_Y) \geq k\tau$  we have

$$\prod_{i=1}^k \lambda_i \geq \exp(k\tau).$$

Let  $\lambda_{\min} = \lambda_k$ . Using  $\sum_{i=1}^{k-1} \lambda_i \leq \text{tr}(\Sigma_Y) - \lambda_k \leq m$ , the AM–GM inequality yields

$$\prod_{i=1}^{k-1} \lambda_i \leq \left( \frac{\sum_{i=1}^{k-1} \lambda_i}{k-1} \right)^{k-1} \leq \left( \frac{m}{k-1} \right)^{k-1}.$$

Therefore

$$\exp(k\tau) \leq \prod_{i=1}^k \lambda_i = \lambda_k \prod_{i=1}^{k-1} \lambda_i \leq \lambda_k \left( \frac{m}{k-1} \right)^{k-1},$$

so

$$\lambda_{\min}(\Sigma_Y) = \lambda_k \geq \exp(k\tau) \frac{(k-1)^{k-1}}{m^{k-1}}.$$

### B.2.14 Proof of Theorem A.14

Let  $\lambda_1 \geq \dots \geq \lambda_k > 0$  be eigenvalues of  $\Sigma$  and  $c = \sum_i \lambda_i$ . The PR constraint implies

$$\text{PR}(\Sigma) = \frac{(\sum_i \lambda_i)^2}{\sum_i \lambda_i^2} \geq r_0 \quad \Rightarrow \quad \sum_{i=1}^k \lambda_i^2 \leq \frac{c^2}{r_0}.$$

Since  $\lambda_{\max}^2 = \lambda_1^2 \leq \sum_i \lambda_i^2$ , we get

$$\lambda_{\max}(\Sigma) \leq \frac{c}{\sqrt{r_0}}.$$

Next, the log-det constraint implies

$$\prod_{i=1}^k \lambda_i = \det(\Sigma) \geq \exp(k\tau).$$

Using  $\lambda_i \leq \lambda_{\max}$  for  $i = 1, \dots, k-1$  gives

$$\exp(k\tau) \leq \lambda_{\min} \lambda_{\max}^{k-1}, \quad \text{so} \quad \lambda_{\min} \geq \frac{\exp(k\tau)}{\lambda_{\max}^{k-1}} \geq \exp(k\tau) \left( \frac{\sqrt{r_0}}{c} \right)^{k-1}.$$

### B.2.15 Proof of Proposition A.16

By Theorem A.4,  $\Phi_\phi^{(K)}$  is a  $C^1$  diffeomorphism with  $|\det(D\Phi_\phi^{(K)}(s))| = 1$  for all  $s$ . For any measurable  $\mathcal{U}$  with finite volume, the change-of-variables theorem gives

$$\text{Vol}(\Phi_\phi^{(K)}(\mathcal{U})) = \int_{\mathcal{U}} |\det(D\Phi_\phi^{(K)}(s))| ds = \int_{\mathcal{U}} 1 ds = \text{Vol}(\mathcal{U}).$$

Hence  $\text{Vol}(\mathcal{U}) > 0$  implies  $\text{Vol}(\Phi_\phi^{(K)}(\mathcal{U})) > 0$ . Therefore the predictor cannot map a positive-volume set to a zero-volume set; any collapse to a lower-volume region must already be present in the encoder outputs.

## C Supplementary theory: maximum entropy on phase space and symplectic factorization

**Theorem C.1** (Maximum entropy on phase space under an expected energy constraint). *Let  $\mathcal{H} : \mathbb{R}^m \rightarrow \mathbb{R}$  be measurable and assume there exists  $\beta > 0$  such that the partition function*

$$Z(\beta) := \int_{\mathbb{R}^m} e^{-\beta\mathcal{H}(s)} ds$$

is finite. Fix  $c \in \mathbb{R}$  and consider the set of densities

$$\mathcal{P}_c := \left\{ p \text{ density on } \mathbb{R}^m : \int p(s) ds = 1, \int \mathcal{H}(s)p(s) ds = c, h(p) > -\infty \right\},$$

where  $h(p) := -\int p \log p$  is differential entropy. If there exists  $\beta^* > 0$  such that  $\mathbb{E}_{p_{\beta^*}}[\mathcal{H}(S)] = c$  for

$$p_{\beta}(s) = \frac{1}{Z(\beta)} e^{-\beta \mathcal{H}(s)},$$

then the unique maximizer of  $h(p)$  over  $\mathcal{P}_c$  is  $p^* = p_{\beta^*}$ .

*Proof.* Fix  $\beta > 0$  with  $Z(\beta) < \infty$  and define  $p_{\beta}(s) = Z(\beta)^{-1} e^{-\beta \mathcal{H}(s)}$ . For any  $p \in \mathcal{P}_c$ ,

$$\text{KL}(p||p_{\beta}) = \int p(s) \log \frac{p(s)}{p_{\beta}(s)} ds \geq 0,$$

with equality iff  $p = p_{\beta}$  a.e. Expanding  $\log p_{\beta}(s) = -\beta \mathcal{H}(s) - \log Z(\beta)$  gives

$$\begin{aligned} \text{KL}(p||p_{\beta}) &= \int p \log p ds - \int p \log p_{\beta} ds \\ &= -h(p) - \int p(s) (-\beta \mathcal{H}(s) - \log Z(\beta)) ds \\ &= -h(p) + \beta \underbrace{\int \mathcal{H}(s)p(s) ds}_{=c} + \log Z(\beta) \underbrace{\int p(s) ds}_{=1} \\ &= -h(p) + \beta c + \log Z(\beta). \end{aligned}$$

Thus  $h(p) \leq \beta c + \log Z(\beta)$  for all  $p \in \mathcal{P}_c$ , with equality iff  $p = p_{\beta}$ .

If there exists  $\beta^*$  such that  $p_{\beta^*} \in \mathcal{P}_c$  (i.e., it matches the energy constraint), then  $p_{\beta^*}$  attains the upper bound and is therefore a maximizer. Uniqueness follows from the equality condition for KL divergence.  $\square$

**Corollary C.2** (Energy-based densities are invariant under Hamiltonian flow). *Let  $\mathcal{H} \in C^2(\mathbb{R}^{2d_0})$  and let  $\Phi_t$  be the Hamiltonian flow of  $\dot{s} = J\nabla \mathcal{H}(s)$ , assumed to be a  $C^1$  diffeomorphism for the times of interest. If  $S$  has density  $p(s) = g(\mathcal{H}(s))$  for some measurable  $g : \mathbb{R} \rightarrow \mathbb{R}_+$ , then for all  $t$ ,  $\Phi_t(S) \stackrel{d}{=} S$ . In particular, the Gibbs density  $p(s) \propto e^{-\beta \mathcal{H}(s)}$  is invariant.*

*Proof.* Energy is conserved along Hamiltonian trajectories: if  $s(t) = \Phi_t(s_0)$ , then

$$\frac{d}{dt} \mathcal{H}(s(t)) = \nabla \mathcal{H}(s(t))^\top \dot{s}(t) = \nabla \mathcal{H}(s(t))^\top J \nabla \mathcal{H}(s(t)) = 0,$$

since  $J^\top = -J$  implies  $u^\top J u = 0$  for all  $u$ . Thus  $\mathcal{H}(\Phi_t(s)) = \mathcal{H}(s)$ .

Also Hamiltonian flows are volume-preserving (Liouville):  $|\det(D\Phi_t(s))| = 1$  for all  $s, t$ . Let  $Y = \Phi_t(S)$ . By change of variables,

$$p_Y(y) = p(\Phi_{-t}(y)) \cdot |\det(D\Phi_{-t}(y))| = g(\mathcal{H}(\Phi_{-t}(y))) \cdot 1 = g(\mathcal{H}(y)) = p(y).$$

Hence  $Y$  and  $S$  have the same density.  $\square$

**Proposition C.3** (Generic kick–drift–scaling factorization of linear symplectic maps). *Let  $A = \begin{pmatrix} a & b \\ c & d \end{pmatrix} \in \text{Sp}(2d_0)$  and assume the block  $d \in \mathbb{R}^{d_0 \times d_0}$  is invertible. Define*

$$B := b d^{-1}, \quad C := d^{-1} c.$$

*Then  $B$  and  $C$  are symmetric and*

$$A = \underbrace{\begin{pmatrix} I & B \\ 0 & I \end{pmatrix}}_{\text{upper shear (drift)}} \underbrace{\begin{pmatrix} d^{-\top} & 0 \\ 0 & d \end{pmatrix}}_{\text{symplectic scaling}} \underbrace{\begin{pmatrix} I & 0 \\ C & I \end{pmatrix}}_{\text{lower shear (kick)}}.$$

*Proof.* Since  $A \in \text{Sp}(2d_0)$ , it satisfies  $A^\top JA = J$ , which implies the standard block identities  $b^\top d = d^\top b$  and  $a^\top d - c^\top b = I$ . From  $b^\top d = d^\top b$  and invertibility of  $d$ ,

$$B^\top = (bd^{-1})^\top = d^{-\top} b^\top = bd^{-1} = B,$$

so  $B$  is symmetric.

Similarly,  $AJA^\top = J$  also holds for symplectic  $A$ , and its block identities include  $cd^\top = dc^\top$ . Then

$$C^\top = (d^{-1}c)^\top = c^\top d^{-\top} = d^{-1}c = C,$$

so  $C$  is symmetric.

Now multiply the three proposed factors:

$$\begin{pmatrix} I & B \\ 0 & I \end{pmatrix} \begin{pmatrix} d^{-\top} & 0 \\ 0 & d \end{pmatrix} \begin{pmatrix} I & 0 \\ C & I \end{pmatrix} = \begin{pmatrix} d^{-\top} + BdC & Bd \\ dC & d \end{pmatrix}.$$

The bottom-right block matches  $d$ . The top-right block matches  $b$  because  $Bd = (bd^{-1})d = b$ . The bottom-left block matches  $c$  because  $dC = d(d^{-1}c) = c$ .

For the top-left block, use the symplectic identity  $ad^\top - bc^\top = I$  (from  $AJA^\top = J$ ) and right-multiply by  $d^{-\top}$ :

$$a - bc^\top d^{-\top} = d^{-\top}.$$

Using  $c^\top d^{-\top} = (d^{-1}c)^\top = C^\top = C$ , this becomes

$$a = d^{-\top} + bC = d^{-\top} + (Bd)C = d^{-\top} + BdC,$$

which matches the computed top-left block. Hence the factorization holds.  $\square$

## D Further results and figures

We refer to the method uniformly as *HamJEPa*; in the code/config files, the suffix `hjepa_mv` simply denotes the minimal multi-view implementation used in our experiments.

### D.1 Frozen-feature diagnostic summaries

Figures 1 (CIFAR-100) and 3 (ImageNet-100) summarize the geometry and non-parametric usefulness of *frozen* encoder representations for the SIGReg baseline and HamJEPa latent states. Each method panel contains four diagnostics computed on *raw* encoder features (i.e., no whitening or other post-processing):

1.  **$k$ NN sweep:** top-1 accuracy as a function of neighborhood size  $k$ .
2. **Covariance eigenspectrum:** top-256 eigenvalues (log-scale) of the *mean-centered* empirical covariance.
3. **Random-pair cosine similarities:** histogram of cosine similarities after per-vector  $\ell_2$  normalization *without* mean subtraction.
4. **Feature norms:** histogram of  $\ell_2$  feature norms.

A key subtlety is that the covariance spectrum is computed after *mean-centering*, whereas the cosine histogram is computed on normalized features *without* centering. Consequently, strongly positive random-pair cosines can arise from a dominant *mean direction* even when the mean-centered covariance remains high-rank. We exploit this complementarity in the discussions below.

### D.2 Discussion CIFAR-100

#### D.2.1 30 epoch results

These results are for the 30 epoch pretraining.

**(1) Neighborhood quality:  $k$ NN sweeps.** In Fig. 1a, the SIGReg baseline peaks at small  $k$  and degrades as  $k$  grows, consistent with semantics being locally present but becoming less class-pure as neighborhoods expand. Quantitatively, SIGReg peaks at  $27.46 \pm 0.31\%$  (at  $k=1$ ) and falls to  $23.10 \pm 0.32\%$  (at  $k=200$ ).

HamJEPA improves the entire sweep for all latent variants in Fig. 1. Notably, the *single*  $q$  state (1024-D) outperforms the SIGReg baseline (2048-D) across the plotted  $k$  values:  $31.45 \pm 0.27\%$  at  $k=20$  for  $q$ , versus  $26.56 \pm 0.18\%$  for SIGReg at  $k=20$  (a  $+4.88 \pm 0.11$  point gain). The  $p$  and  $(q, p)$  variants achieve  $29.71 \pm 0.25\%$  and  $30.88 \pm 0.39\%$  at  $k=20$ , respectively. That  $(q, p)$  does not exceed  $q$  suggests that, under the default weighting,  $p$  contributes less additional *metric-consistent* neighborhood structure than  $q$ , even though it remains informative for linear decoding (see below).

**(2) Linear probe vs.  $k$ NN: separability without neighborhood purity.** While  $k$ NN distinguishes the latent variants, the linear probe largely does not: SIGReg reaches  $30.43 \pm 0.30\%$  top-1, whereas HamJEPA reaches  $33.95 \pm 0.24\%$ ,  $33.07 \pm 0.36\%$  and  $34.18 \pm 0.17\%$  top-1 for  $q$ ,  $p$ , and  $(q, p)$  respectively. A useful interpretation is that  $p$  is *linearly* discriminative but induces less clean neighborhoods under the raw metric, so its gains show up more clearly in the probe than in  $k$ NN.

**(3) Covariance eigenspectrum: rank proxies and collapse checks.** The top-right panels show mean-centered covariance spectra (top 256 eigenvalues, log-scale). A convenient summary is the effective-rank proxy computed from these eigenvalues: SIGReg has effective rank  $\approx 109.73 \pm 0.61$  (top-256), whereas HamJEPA- $q$  increases to  $125.58 \pm 3.33$ . In contrast, HamJEPA- $p$  is more concentrated (effective rank  $79.46 \pm 3.99$ ), and  $(q, p)$  lies in between ( $93.10 \pm 4.00$ ). Two points follow: (i) HamJEPA- $q$  does *not* achieve its downstream gain via low-rank collapse (the centered covariance is high-rank), and (ii) the  $q/p$  split is geometrically meaningful:  $q$  and  $p$  allocate variance differently even when their linear probe scores are similar.

**(4) Cosine similarities: diagnosing mean-dominance.** The bottom-left panels reveal the largest qualitative difference. SIGReg’s random-pair cosines are centered near zero (mean  $0.01699 \pm 0.00089$ ) with substantial negative mass, which is consistent with its isotropy-encouraging design.

HamJEPA’s cosines shift sharply positive: mean cosine is  $0.71561 \pm 0.00129$  for  $q$ ,  $0.61687 \pm 0.00409$  for  $p$ , and  $0.66613 \pm 0.00270$  for  $(q, p)$ . Crucially, this strong alignment coexists with a *high-rank mean-centered covariance* (especially for  $q$ ). This combination is most naturally explained by a large *non-zero mean feature direction* that dominates dot products when features are not explicitly centered: the covariance spectrum removes that mean direction by construction, while the cosine histogram does not. In other words, the CIFAR-100 HamJEPA embeddings look “cone-like” in raw normalized space primarily due to mean-dominance rather than variance collapse.

**(5) Feature norms: scale control and the  $(q, p)$  energy split.** SIGReg feature norms are concentrated around  $44.891 \pm 0.090$ , whereas HamJEPA’s  $q$  and  $p$  have smaller typical norms around  $31.358 \pm 0.017$  and  $31.281 \pm 0.029$ . The concatenated  $(q, p)$  norm shifts back to  $44.303 \pm 0.027$ , closely matching the Pythagorean combination  $\|[q; p]\|_2 \approx \sqrt{\|q\|_2^2 + \|p\|_2^2}$ , which is what one expects if  $q$  and  $p$  maintain comparable energy rather than one collapsing to near-zero. This provides a simple consistency check that the phase-space parameterization retains a balanced contribution from both coordinates.

## D.2.2 80 epoch results

By design, the CIFAR-100 pretraining curves tend to plateau because the experiment is set up as a minimal, controlled training regime, whose goal is to isolate representational geometry effects rather than to chase absolute accuracy with an aggressively optimized recipe. CIFAR-100 is small and low-resolution, so the encoder typically learns the dominant semantic invariances early; after that point, additional epochs mainly yield diminishing returns (small refinements in neighborhood structure or feature scaling) that often do not translate into large gains in linear-probe/ $k$ NN top-1 under a fixed evaluation protocol. In other words, once both methods reach a “good-enough” feature space, the remaining headroom is mostly governed by recipe choices we intentionally avoid here (stronger augmentation, longer schedules, larger models, distillation/EMA, more hyperparameter search), since those would confound the attribution: we want any observed differences to come primarily from the geometry induced by the training dynamics, not from extra optimization budget.

Method	Variant	Linear probe (%)	$k$ NN@20 (%)	$k$ NN best (%)
SIGReg	single	33.95	27.98	28.71 @ $k=1$
MLP-HJEPA (non-symplectic)	$q$	42.26	28.10	28.10 @ $k=20$
MLP-HJEPA (non-symplectic)	$p$	41.90	28.30	28.30 @ $k=20$
MLP-HJEPA (non-symplectic)	$(q, p)$	42.77	28.15	28.15 @ $k=20$
HamJEPA (symplectic)	$q$	44.59	34.43	34.43 @ $k=20$
HamJEPA (symplectic)	$p$	44.44	32.96	32.96 @ $k=20$
HamJEPA (symplectic)	$(q, p)$	44.52	33.66	33.66 @ $k=20$

Table 3: **CIFAR-100, 80-epoch predictor-family ablation.** MLP-HJEPA keeps the phase-space encoder, channel-wise  $q/p$  split, identity projector, prediction loss, anti-collapse regularizers, optimizer, batch size, and 80-epoch schedule fixed, and replaces only the symplectic leapfrog predictor by a non-symplectic residual MLP predictor.

**Predictor-family ablation: what changes and what stays fixed.** In addition to SIGReg and symplectic HamJEPA, we evaluate a non-symplectic predictor ablation, *MLP-HJEPA*, that keeps the phase-space encoder, channel-wise  $q/p$  split, identity projector, prediction loss, anti-collapse regularizers, optimizer, batch size, and training schedule fixed, and replaces only the leapfrog Hamiltonian rollout by a generic residual MLP rollout predictor. Because Fig. 2 visualizes only SIGReg and symplectic HamJEPA, we summarize the MLP ablation numerically in Table 3. This is therefore a clean apples-to-apples test of whether the gains come mainly from the phase-space representation and encoder-side regularization, or from the symplectic predictor itself.

**(1) Neighborhood quality:  $k$ NN sweeps and local semantic structure.** At 80 epochs, SIGReg reaches 27.98% at  $k$ NN@20 and peaks at 28.71% over the full sweep (at  $k=1$ ). It peaks at small  $k$  and degrades as  $k$  grows, consistent with semantics being locally present but becoming less class-pure as neighborhoods expand. The non-symplectic MLP-HJEPA ablation barely changes this picture: its best  $k$ NN@20 is only 28.30% (from the  $p$  readout), a gain of just +0.32 points over SIGReg, and its best-over- $k$  score is in fact slightly *below* SIGReg (28.30% vs. 28.71%). By contrast, symplectic HamJEPA is qualitatively different: the  $q$  readout reaches 34.43% at  $k$ NN@20 and also attains the best-over- $k$  value of 34.43% (at  $k=20$ ), namely gains of +6.45 points at  $k$ NN@20 and +5.72 points best-over- $k$  relative to SIGReg. Notably, the *single*  $q$  state (1024-D) outperforms the SIGReg baseline (2048-D) across the plotted  $k$  values. Best-vs.-best, the symplectic predictor outperforms the MLP predictor by +6.13 points at  $k$ NN@20. This is the sharpest evidence that the symplectic rollout is doing something specifically geometric: the phase-space encoder alone does *not* automatically produce high-purity local neighborhoods.

**(2) Linear probe: phase-space structure already helps, but symplecticity still matters.** The linear-probe comparison is more nuanced. MLP-HJEPA already substantially outperforms SIGReg, reaching 42.77% top-1 in its best variant ( $(q, p)$ ) versus 33.95% for SIGReg, a gain of +8.82 points. Symplectic HamJEPA pushes this further to 44.59% (best  $q$  readout), i.e. another +1.82 points over MLP-HJEPA and +10.64 over SIGReg. This suggests that a large part of the linear-separability gain comes from the *phase-space parameterization plus encoder-side anti-collapse bridge*, not only from symplecticity. However, once nonparametric neighborhood quality is examined, the predictor family becomes decisive: the MLP predictor narrows much of the probe gap, but essentially none of the  $k$ NN gap.

**(3)  $q/p$  decomposition: structured phase space versus generic feature blocks.** Within MLP-HJEPA, the three readouts are almost indistinguishable: linear probe is 42.26%/41.90%/42.77% for  $q/p/(q, p)$ , and  $k$ NN@20 is 28.10%/28.30%/28.15%. In other words, once the symplectic predictor is removed, the  $q/p$  split behaves much more like a generic two-block partition of the feature vector than like a structured position-momentum state space. This contrasts with symplectic HamJEPA, where  $q$  is the cleanest neighborhood readout,  $p$  is slightly weaker, and  $(q, p)$  remains close but does not dominate. The natural interpretation is that the Hamiltonian rollout induces a genuine functional differentiation between the two coordinates, whereas the MLP rollout does not.

**(4) Mean-centered covariance geometry: high-rank symplectic  $q$  versus concentrated MLP states.** The scalar covariance diagnostics sharpen this distinction. SIGReg has effective rank  $\approx 99.80$  and participation ratio  $\approx 58.32$  on the top-256 eigenspectrum. Symplectic HamJEP- $q$  is substantially broader still, with effective rank  $\approx 128.98$  and participation ratio  $\approx 70.34$ , confirming that its downstream gains are *not* coming from collapse onto a narrow subspace. By contrast, MLP-HJEP- $q$  is much more spectrally concentrated: its effective rank is only  $\approx 42.06$  for  $q$ ,  $\approx 43.95$  for  $p$ , and  $\approx 42.85$  for  $(q, p)$ , with participation ratios only  $\approx 23.65$ – $24.99$ . So although the MLP ablation yields good linear-probe accuracy, it does so with a much more concentrated mean-centered covariance geometry than symplectic HamJEP- $q$ . Put differently: the MLP predictor can produce a linearly usable representation, but it does not organize a broad, high-rank content geometry in the way the symplectic predictor does.

**(5) Cosine similarities and feature norms: the predictor changes geometry, not just scale.** The random-pair cosine statistics again place MLP-HJEP- $q$  much closer to SIGReg than to symplectic HamJEP- $q$ . SIGReg has cosine mean  $\approx 0.006$  with standard deviation  $\approx 0.121$ , while MLP-HJEP- $q$  remains near zero as well (cosine means  $\approx 0.042$  for  $q$ ,  $\approx 0.053$  for  $p$ , and  $\approx 0.047$  for  $(q, p)$ , all with standard deviation around 0.19). Symplectic HamJEP- $q$ , in contrast, exhibits strongly positive cosine means ( $\approx 0.625$  for  $q$ ,  $\approx 0.443$  for  $p$ , and  $\approx 0.534$  for  $(q, p)$ ), reflecting the markedly more aligned raw geometry visible in Fig. 2. Importantly, this difference is *not* explained by trivial scale effects: the feature norms of MLP-HJEP- $q$  are nearly the same as those of symplectic HamJEP- $q$  (means  $\approx 32.21$ ,  $31.89$ , and  $45.32$  for MLP-HJEP- $q$  versus  $\approx 31.81$ ,  $31.88$ , and  $45.06$  for symplectic HamJEP- $q$ ). Thus the predictor family is primarily changing *how* variance is organized and aligned, not simply how large the features are.

**Takeaway (CIFAR-100, 80 epochs).** The MLP ablation is informative in exactly the right way. It shows that the phase-space encoder,  $q/p$  split, and non-isotropic anti-collapse regularization already explain a large fraction of the linear-probe improvement over SIGReg. However, they do *not* explain the major improvement in nonparametric neighborhood quality. That gain appears to be specifically tied to the symplectic predictor: relative to the non-symplectic MLP rollout, symplectic HamJEP- $q$  produces much better  $k$ NN structure, a broader and less concentrated mean-centered covariance for the content coordinate, and a more distinctive raw embedding geometry. In this sense, the symplectic component is not merely a mild architectural preference; it is the ingredient that turns a linearly useful phase-space representation into one with substantially cleaner local semantic geometry.

### D.3 Discussion ImageNet-100

**(1) Frozen-feature quality:  $k$ NN and probe.** On ImageNet-100, HamJEP- $q$  again improves non-parametric and linear evaluation. In Fig. 3, the dimension-matched comparison (2048-D) is SIGReg  $(q, p)$  versus HamJEP- $(q, p)$ . At the final checkpoint, SIGReg  $(q, p)$  reaches a best  $k$ NN top-1 of 21.7% (peak near  $k=50$ ), whereas HamJEP- $(q, p)$  reaches 25.9% (a +4.2 point gain). For linear probing, SIGReg  $(q, p)$  reaches 25.5% top-1, whereas HamJEP- $(q, p)$  reaches 32.0% (a +6.5 point gain).

Figure 5 additionally provides a strict 1024-D comparison on  $q$ : at epoch 45, HamJEP- $q$  improves linear probe by +7.52 points and best  $k$ NN by +4.90 points over SIGReg- $q$  (as annotated).

**(2) Covariance rank: HamJEP- $q$  spreads variance across many directions.** The covariance spectra (top-right) and the effective-rank proxy show a stark contrast: SIGReg- $q$  and SIGReg- $p$  have low effective rank ( $\approx 38$ – $39$  on the top-256 eigenvalues), whereas HamJEP- $q$  and HamJEP- $p$  are much higher ( $\approx 95$ – $98$ ). Thus, on ImageNet-100, HamJEP- $q$ 's gains are associated with *more* variance being spread across principal directions (higher rank), not less.

**(3) Cosine similarities: mild global alignment without extreme cone structure.** Unlike CIFAR-100, ImageNet-100 does *not* show an extreme cone effect for HamJEP- $q$ . SIGReg's random-pair cosines remain centered near zero (mean  $\approx 0$ ), while HamJEP- $q$  shifts to moderately positive cosines (mean  $\approx 0.27$ – $0.28$  depending on  $q/p/(q, p)$ ). Given the simultaneously high effective rank of the mean-centered covariance, this again suggests a shared direction and/or non-zero mean, but the effect is substantially weaker than on CIFAR-100.

**(4)  $q/p$  decomposition: complementarity for SIGReg, redundancy for HamJEPa.** Figure 4 makes the structural difference explicit. For SIGReg+tokens,  $(q, p)$  is consistently best throughout training, indicating that  $q$  and  $p$  halves are not individually sufficient but become competitive when concatenated. For HamJEPa,  $q$  and  $p$  are individually as strong as  $(q, p)$  (both for probe and  $k$ NN), suggesting that both coordinates carry similar semantic content and that concatenation adds little.

**(5) Dynamics: accuracy tracks geometry for HamJEPa, not for SIGReg.** In Fig. 5, HamJEPa’s effective rank increases over training while probe accuracy improves, yielding a strong positive association in the probe-versus-rank plot (annotated  $\rho$ ). SIGReg shows the opposite: effective rank decreases while accuracy rises slightly, yielding a negative association. This supports the interpretation that HamJEPa’s ImageNet gains co-occur with a progressively less concentrated (mean-centered) covariance structure.

**Takeaway (ImageNet-100).** On ImageNet-100, HamJEPa improves  $k$ NN and linear probing while producing substantially higher-rank mean-centered covariance than SIGReg and only moderately more positive cosine alignment. In contrast to SIGReg+tokens, HamJEPa makes both  $q$  and  $p$  individually strong, with little benefit from concatenation.

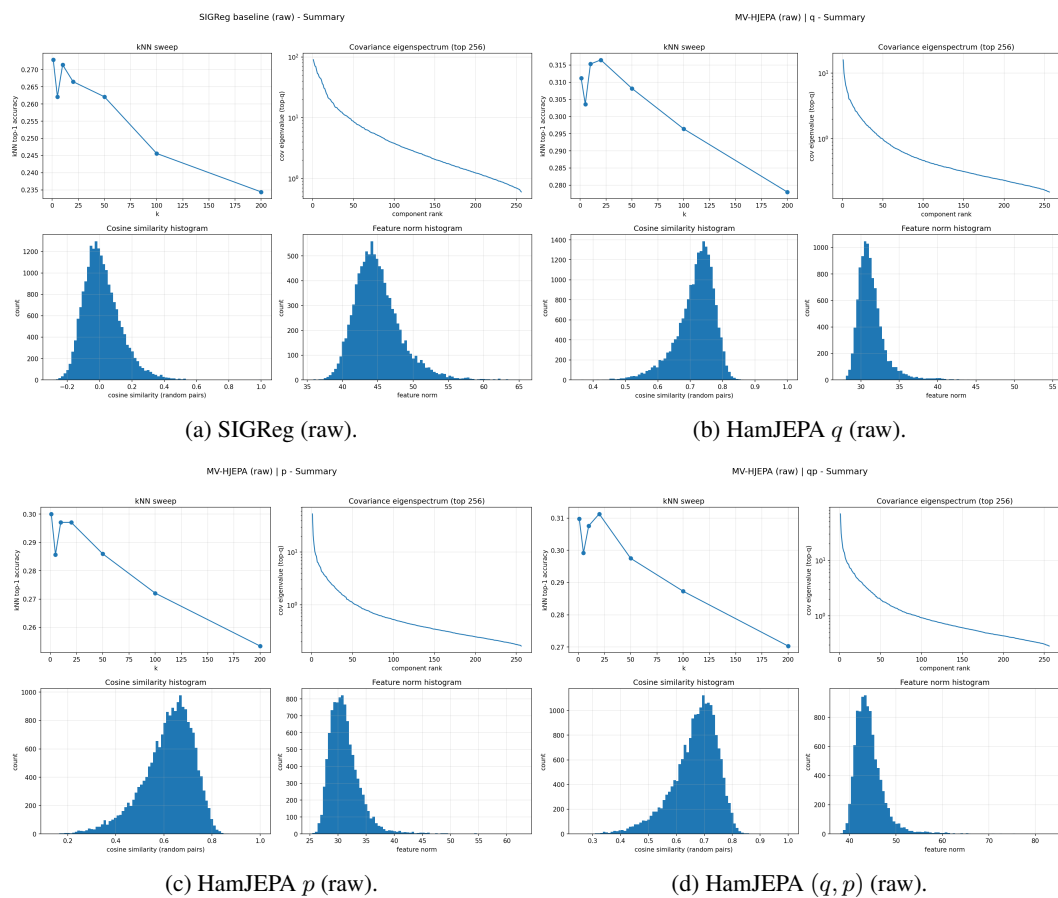


Figure 1: **Frozen-feature diagnostic summaries (raw) 30 epochs.** Each panel contains: (top-left)  $k$ NN sweep; (top-right) covariance eigenspectrum (top 256, log scale); (bottom-left) cosine similarity histogram (random pairs); (bottom-right) feature norm histogram.

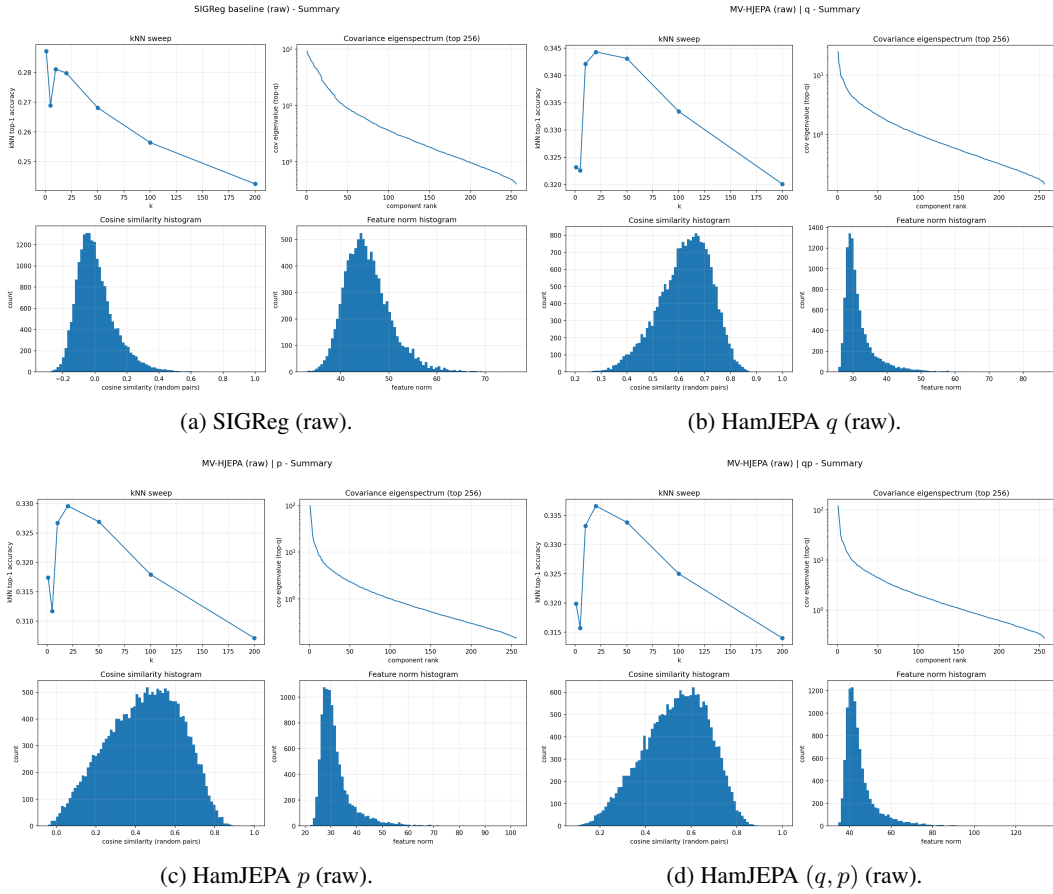


Figure 2: **CIFAR-100 frozen-feature diagnostic summaries (raw) 80 epochs**. Each panel contains: (top-left)  $k$ NN sweep; (top-right) mean-centered covariance eigenspectrum (top 256, log scale); (bottom-left) random-pair cosine similarity histogram; (bottom-right) feature norm histogram.

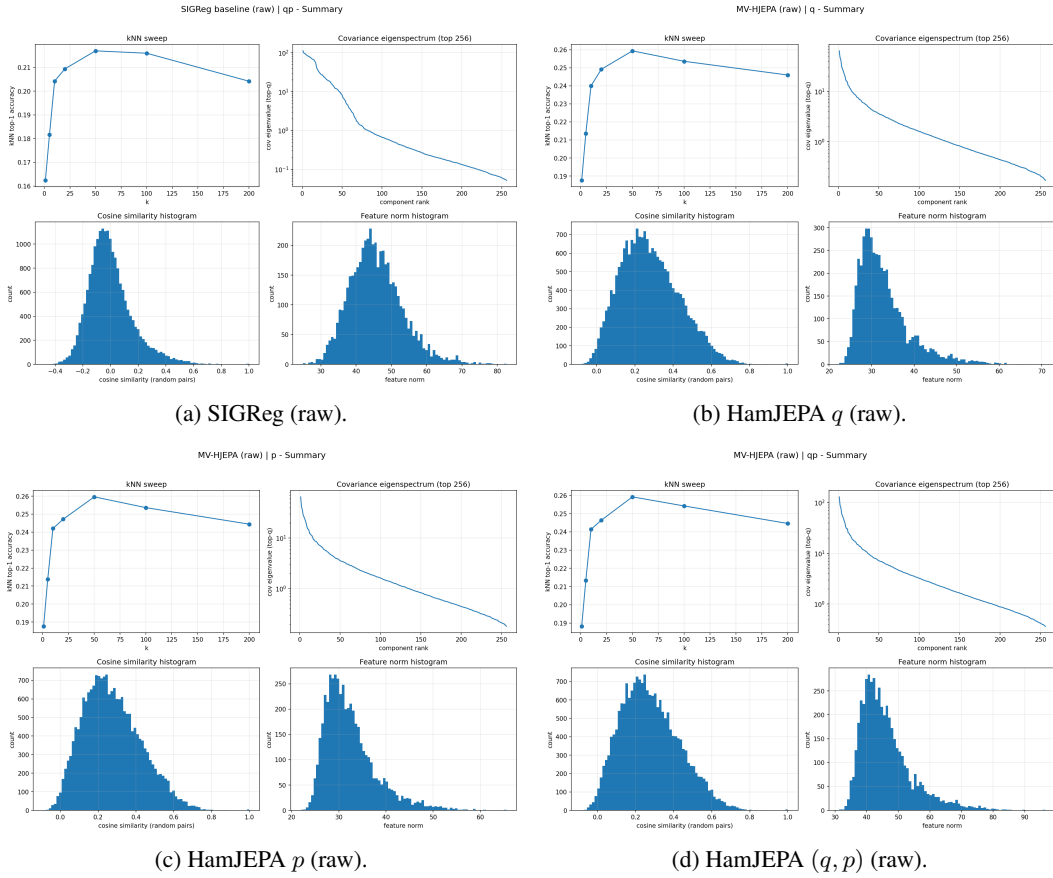


Figure 3: **ImageNet-100 frozen-feature diagnostic summaries (raw)**. Each panel contains: (top-left)  $k$ NN sweep; (top-right) covariance eigenspectrum (top 256, log scale); (bottom-left) cosine similarity histogram (random pairs); (bottom-right) feature norm histogram.

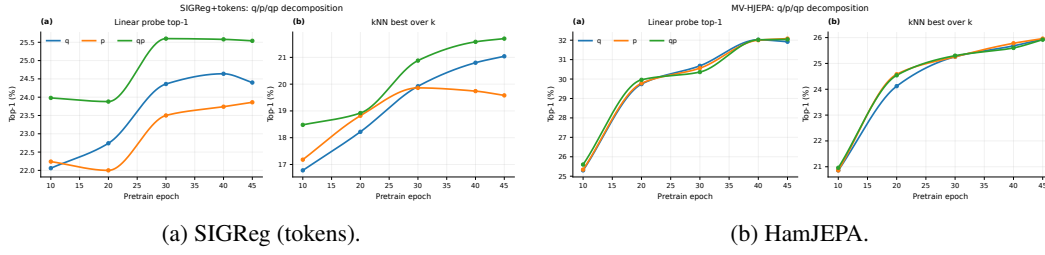


Figure 4:  $q/p$  decomposition across pretraining (ImageNet-100). We evaluate frozen features extracted at sparse pretraining checkpoints using (left) a linear probe top-1 and (right) the best  $k$ NN top-1 across the evaluated  $k$  values. For SIGReg+tokens, concatenating  $(q, p)$  is consistently better than either half alone, indicating that the split halves are complementary (and/or that doubling feature dimension helps). For HamJEPa,  $q$ ,  $p$ , and  $(q, p)$  track each other closely, suggesting that both phase-space coordinates are individually informative and largely redundant under the symplectic objective. (Left) SIGReg tokens. (Right) HamJEPa.

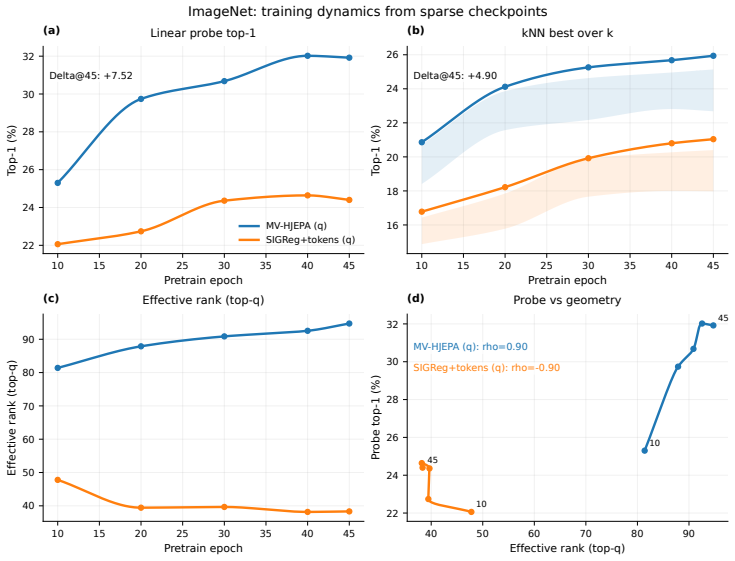


Figure 5: **ImageNet-100 training dynamics from sparse checkpoints (geometry vs. accuracy).** Using the  $q$  representation at a set of pretraining epochs, we plot: (a) linear probe top-1; (b) best  $k$ NN top-1 over  $k$  (shaded region indicates the spread over the  $k$  sweep); (c) effective-rank proxy computed from the top-256 eigenvalues of the mean-centered  $q$  covariance; (d) probe accuracy versus effective rank (points annotated by epoch), with the plotted correlation coefficient  $\rho$ . HamJEPa improves steadily and shows increasing effective rank, while SIGReg+tokens improves modestly while its effective rank decreases; the deltas at epoch 45 are annotated in panels (a,b).

## D.4 Further figures

Figures 6–8 provide an intuition for a LeJEPA-inspired *sliced-projection* diagnostic: rather than comparing rollout distributions only in aggregate, we compare many 1D projections (a Cramér–Wold viewpoint) to expose direction-dependent geometric distortion.

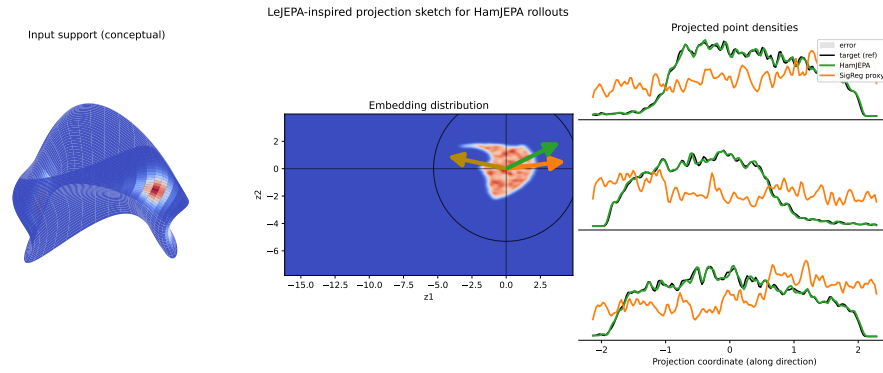


Figure 6: **LeJEPA-inspired sliced-projection diagnostic for HamJEPA rollouts (cartoon)**. Left: conceptual support of the input distribution (manifold-structured data). Middle: an example embedding distribution in a 2D slice with several projection directions  $u(\theta)$ . Right: estimated 1D projected densities along representative directions; black denotes the reference/target, green denotes HamJEPA rollouts, orange denotes a SIGReg proxy baseline, and the shaded band visualizes the per-direction projection error. Matching many 1D projections (Cramér–Wold/sliced view) makes geometric distortion from non-structure-preserving dynamics visible, while symplectic rollouts remain close to the reference across directions.

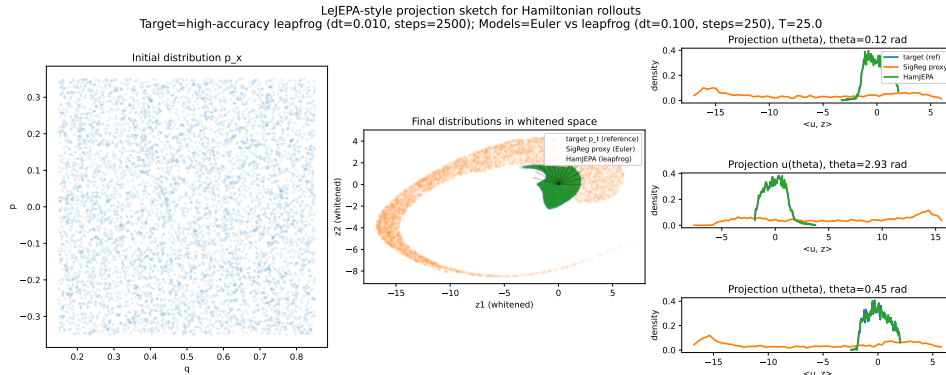


Figure 7: **LeJEPA-style projection sketch on a toy Hamiltonian transport problem**. Left: initial phase-space distribution  $p_x$  over  $(q, p)$ . Middle: final distributions in whitened coordinates after rolling out to a fixed horizon  $T$ ; the reference target is generated by a high-accuracy leapfrog integrator, while the two model curves compare a coarse Euler rollout (SIGReg proxy) against a coarse leapfrog rollout (HamJEPA). Right: 1D densities of projections  $\langle u(\theta), z \rangle$  for representative angles  $\theta$ , showing that leapfrog-based rollouts track the reference distribution across directions, whereas Euler produces large direction-dependent mismatch.

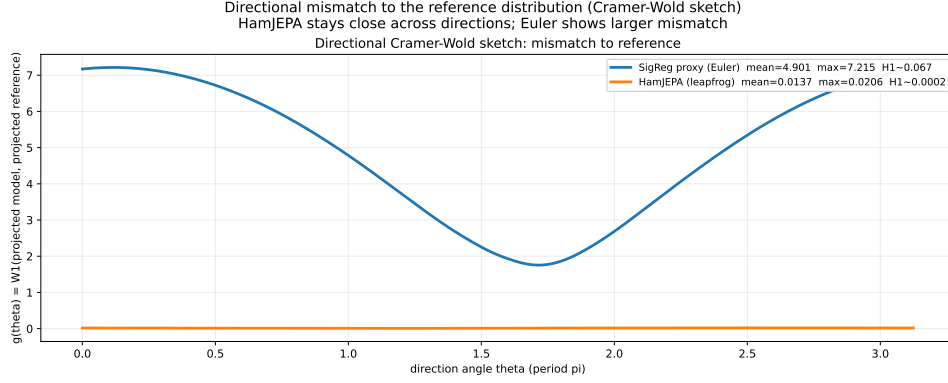


Figure 8: **Directional Cramér–Wold discrepancy (sliced mismatch) versus projection angle.** For each direction angle  $\theta$  (period  $\pi$ ), we compute a 1D mismatch  $g(\theta) = W_1(\langle u(\theta), Z_{\text{model}} \rangle, \langle u(\theta), Z_{\text{ref}} \rangle)$  between the projected model and reference distributions. HamJEPA (leapfrog) stays uniformly close across directions, while the Euler/SIGReg proxy exhibits large, anisotropic deviation; the legend reports summary statistics over  $\theta$  (mean/max and the aggregate score used in the plot).

## E A visual guide to HamJEPA

This appendix gives a diagrammatic explanation of HamJEPA for readers who want a more visual account than the equation-level presentation in the main text. The figures here are explanatory schematics rather than empirical results. Their purpose is to separate the method into four conceptual layers: (i) the overall two-view prediction pipeline, (ii) how the encoder constructs the phase-space state  $s = [q; p]$ , (iii) how the predictor evolves that state by a symplectic Hamiltonian rollout, and (iv) why encoder-side anti-collapse regularization is still required even when the predictor itself is symplectic.

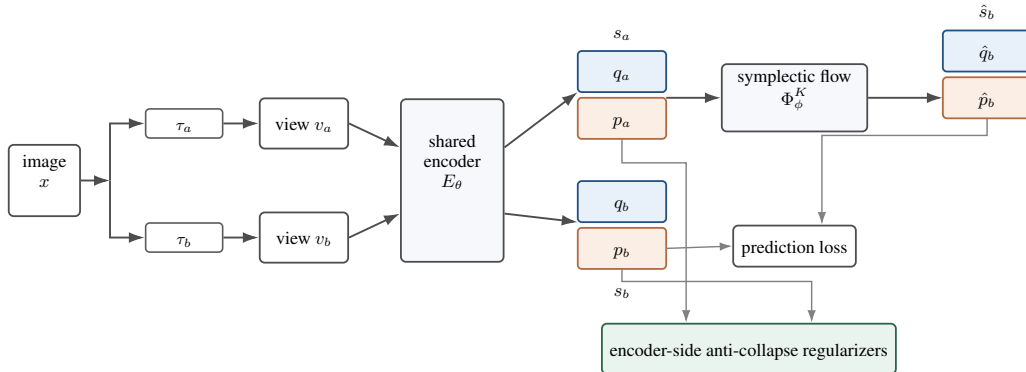


Figure 9: **HamJEPA at the highest level.** Two augmented views of the same image are encoded by a shared encoder into phase-space states  $s_a = [q_a; p_a]$  and  $s_b = [q_b; p_b]$ . The predictor is not an unconstrained regression head: it is a structured Hamiltonian rollout  $\Phi_\phi^K$  that evolves  $s_a$  into a predicted target state  $\hat{s}_b$ . Training combines a prediction loss between  $\hat{s}_b$  and  $s_b$  with separate encoder-side anti-collapse regularizers applied across the batch of states.

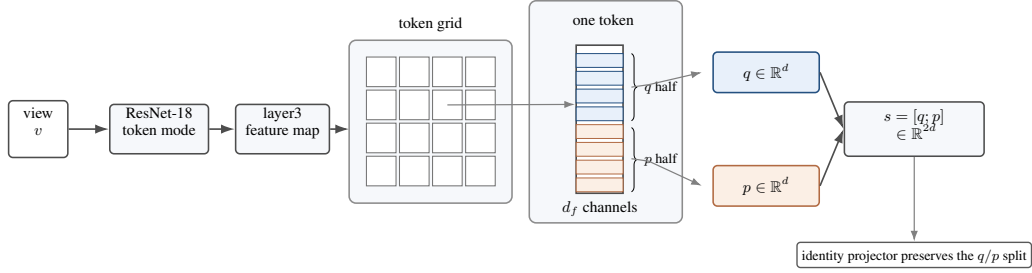


Figure 10: **How the encoder constructs the phase-space state.** HamJEPA is not just taking an arbitrary vector and renaming its halves as  $q$  and  $p$ . In the implementation, the encoder runs in token mode: an intermediate ResNet feature map is converted into a token grid, the *channel stack of each token* is split into a  $q$  half and a  $p$  half, and those halves are flattened across the spatial grid to form  $q \in \mathbb{R}^d$  and  $p \in \mathbb{R}^d$ . These are then concatenated into  $s = [q; p] \in \mathbb{R}^{2d}$ . This is why HamJEPA uses an identity projector: a learned MLP after the encoder would remix the coordinates and destroy the intended  $q/p$  semantics.

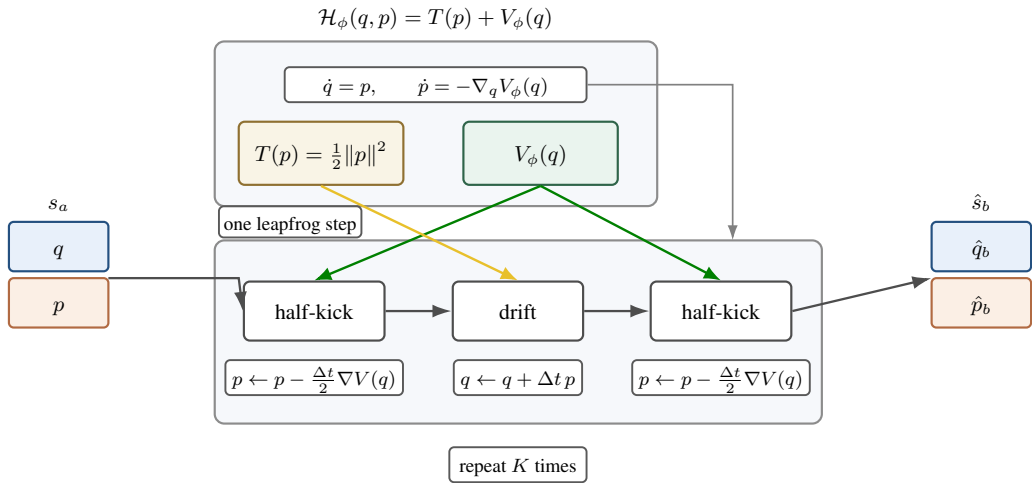


Figure 11: **What the predictor is doing.** HamJEPA does not use an arbitrary predictor  $z_a \mapsto \hat{z}_b$ . Instead, it rolls the state forward with a learned separable Hamiltonian  $\mathcal{H}_\phi(q, p) = T(p) + V_\phi(q)$  and a leapfrog integrator. The potential  $V_\phi(q)$  drives the kick updates through  $\nabla_q V_\phi(q)$ , while the kinetic term  $T(p) = \frac{1}{2} \|p\|^2$  yields the drift update  $q \leftarrow q + \Delta t p$ . Repeating this structured step  $K$  times produces the predicted target state  $\hat{s}_b = \Phi_\phi^K(s_a)$ .

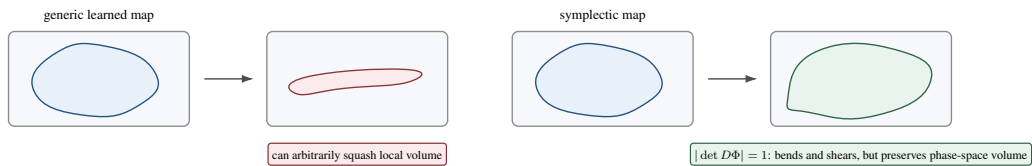


Figure 12: **What “symplectic” means geometrically.** A generic learned map can bend, stretch, and arbitrarily collapse local geometry. A symplectic map can still deform the state space, but it preserves total phase-space volume locally, i.e.  $|\det D\Phi| = 1$ . This gives the predictor a structured notion of reversibility and ensures that the predictor itself is not the source of volume collapse.

Symplecticity constrains the predictor, but it does *not* by itself prevent encoder collapse. A collapsed encoder could still map many different views to almost the same latent state, and a perfectly symplectic predictor would then only move around an already-degenerate state cloud. The next two figures

therefore separate these two roles: first, why predictor structure alone is insufficient; second, how the encoder-side regularizers keep the latent space alive.

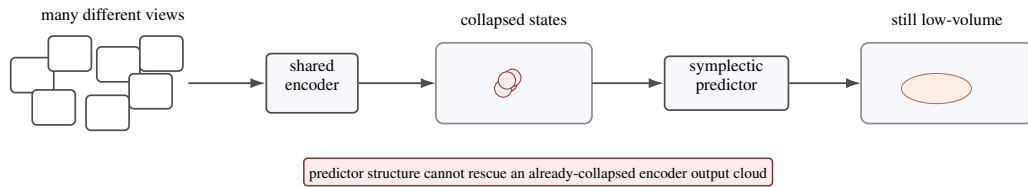


Figure 13: **Why the predictor alone is not enough.** Even if the predictor is perfectly symplectic, the encoder could still map many different views to nearly the same latent state. In that situation the rollout acts on an already-collapsed representation. This is why HamJEPa needs a second component beyond the predictor: encoder-side anti-collapse regularization.

**Why the predictor alone is not enough.** The symplectic constraint belongs to the predictor map, not to the encoder. This means it prevents the rollout from crushing phase-space volume, but it does *not* stop the encoder itself from mapping many different views to nearly the same latent state. A collapsed encoder would therefore still give a degenerate state cloud, even with a perfectly symplectic predictor. The next figures isolate the role of each encoder-side anti-collapse regularizer.

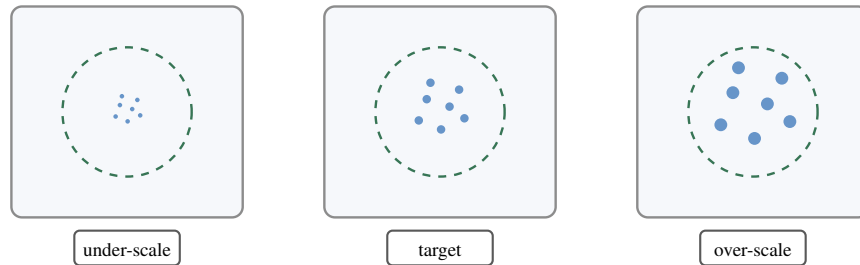


Figure 14: **Energy budget.** The energy budget keeps the average per-dimension scale of  $q$  and  $p$  near a target range. It penalizes both under-scaled states (which risk collapse toward zero) and over-scaled states (which can destabilize dynamics), so the latent cloud stays at a controlled overall radius.

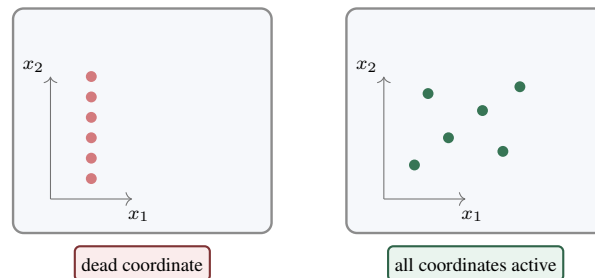


Figure 15: **Variance floor.** The variance floor prevents individual coordinates from becoming nearly constant across the batch. Visually, it revives dead axes: instead of allowing the latent cloud to collapse onto a lower-dimensional direction, it forces each coordinate to retain a minimum amount of variation.

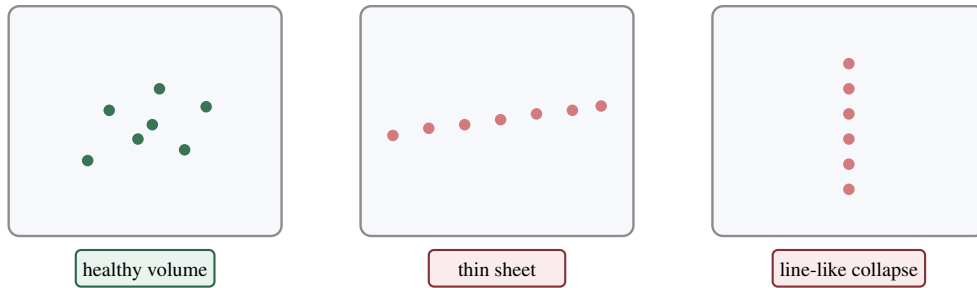


Figure 16: **Projected log-det floor.** The projected log-det floor prevents the batch representation from flattening into a very low-volume set. It does not require isotropy, but it does force the projected covariance to retain nontrivial volume, ruling out extreme degeneracies such as line-like or sheet-like collapse.

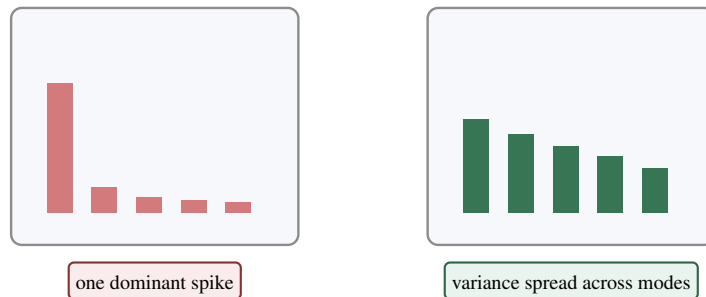


Figure 17: **Participation-ratio floor and top-eigenvalue control.** These penalties prevent the representation from surviving only through one huge dominant direction. The participation-ratio floor encourages variance to remain spread across multiple modes, while the top-eigenvalue ceiling prevents a single spike from taking over the spectrum.

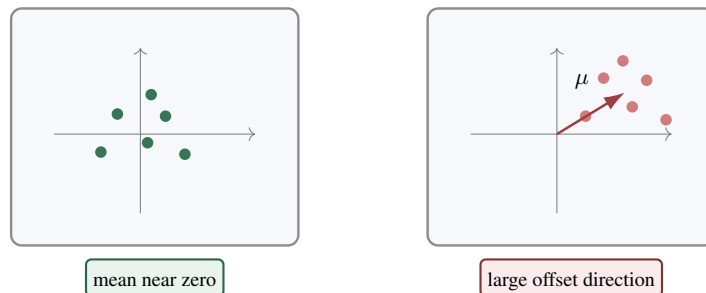


Figure 18: **Mean penalty.** A large global mean can create a dominant offset direction that makes random-pair cosine similarities look artificially cone-like. The mean penalty discourages this by keeping the batch mean closer to zero, so the geometry is not dominated by a single global shift.

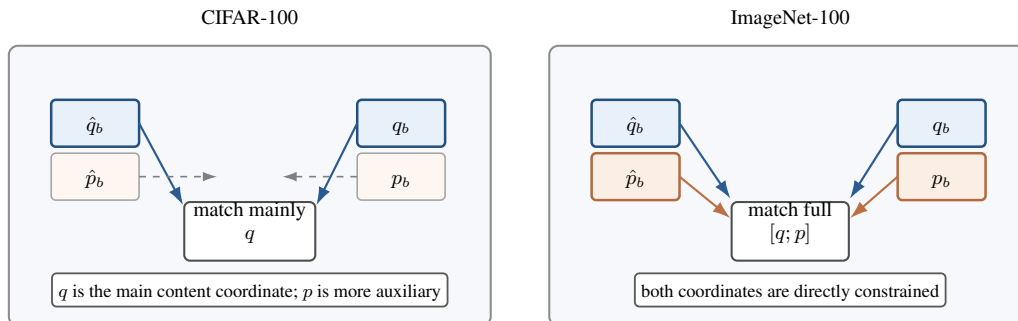


Figure 19: **Why CIFAR-100 and ImageNet-100 use different matching choices.** On CIFAR-100 the training objective emphasizes the content coordinate  $q$ , so  $q$  is the cleanest downstream readout and  $p$  mainly supports the dynamics. On ImageNet-100 the stable regime was to match the full state  $[q; p]$ , which directly constrains both coordinates and makes  $p$  much more informative.

**How to read the sequence.** Taken together, Figs. 9–19 decompose the full method into three conceptual layers: the encoder constructs a structured phase-space state, the predictor evolves that state with a symplectic Hamiltonian rollout, and the regularizers ensure that the encoder supplies a non-degenerate cloud of states for those dynamics to act on. The distinctive point is therefore twofold: HamJEPA changes both the *representation parameterization* (from a single embedding to a phase-space state) and the *predictor family* (from arbitrary regression to Hamiltonian dynamics), while avoiding the need to force the encoder marginal toward Euclidean isotropy.

## F Implementation Details and Algorithms

In this section (as in the code) we refer to *HamJEPA* as *MV-HJEPA*, denoting the minimal multi-view implementation used in our experiments.

### F.1 Compute resources

All reported experiments were run on NVIDIA A100 GPUs. CIFAR-100 pretraining took approximately 40 seconds per epoch, corresponding to roughly 20 minutes for a 30-epoch run and roughly 53 minutes for an 80-epoch run. ImageNet-100 pretraining took approximately 5 hours for a 45-epoch run. Downstream evaluation was also run on A100 GPUs and required under 5 minutes for CIFAR-100 and under 15 minutes for ImageNet-100 per checkpoint/readout evaluation. These timings are approximate wall-clock measurements; peak GPU memory was not separately profiled.

### F.2 Two training modes: MV-HJEPA vs. baseline (LeJEPA + regularizer)

Our training scripts are *mode-switched* by the presence of a `hjepa:` block in the YAML:

- **MV-HJEPA mode** (`hjepa` present): we treat the representation as a phase-space state  $z = [q; p] \in \mathbb{R}^{2d}$  and train a Hamiltonian flow predictor that maps between two global views. We additionally apply scale/diversity regularizers on *all* views.
- **Baseline mode** (`hjepa` absent): we use the *LeJEPA* prediction objective where all views predict the mean of the global views, and we optionally add a distributional regularizer such as SIGReg.

### F.3 Data pipeline and multi-view batching (CIFAR100 vs. ImageNet)

**Multi-crop dataset contract.** Each dataset example yields a list of  $V$  augmented views (multi-crop), plus labels:

$$(\{x^{(v)}\}_{v=1}^V, y, y_{\text{coarse}}).$$

In our configurations, we set `num_global_views=2` and `num_local_views=0`, so  $V = 2$ .

**CIFAR100MultiCrop.** `eval/datasets/cifar100_multicrop.py` applies the full augmentation *in the worker* and returns *float tensors already normalized* (using `ToTensor()` + `Normalize`). Notable defaults:

- `out_size=32` (CIFAR resolution)
- blur uses a small kernel (`kernel_size=3`)

**ImageNetMultiCrop.** `eval/datasets/imagenet_multicrop.py` applies the same high-level augmentation pattern, but returns *uint8 tensors* using `PILToTensor()` to reduce dataloader IPC bandwidth. We then convert to float and normalize *on device* inside the ImageNet training loop. Notable defaults:

- `out_size=224`
- blur uses a larger kernel (`kernel_size=23`) appropriate for higher resolution
- global crop scale defaults match the YAML (`global_scale=[0.4, 1.0]`)

**Multi-view batching optimization.** For computational efficiency, we concatenate views along the batch dimension and run a *single* encoder+projector forward:

$$x_{\text{cat}} = \text{concat}(x^{(1)}, \dots, x^{(V)}) \in \mathbb{R}^{(VB) \times C \times H \times W}, \quad z_{\text{cat}} = P(E(x_{\text{cat}})) \in \mathbb{R}^{(VB) \times K}.$$

We then reshape:

$$z_{\text{views}} \in \mathbb{R}^{V \times B \times K}, \quad z_{\text{views}} = \text{reshape}(z_{\text{cat}}, (V, B, K)).$$

This is exactly how both `train_cifar_hamjepa.py` and `train_imagenet_hamjepa.py` operate.

#### F.4 Encoder and token-state parameterization

**ResNet18 backbone with dataset-specific stem.** We use `torchvision.models.resnet18(weights=None)` and alter the stem depending on the dataset:

- **CIFAR stem** (`encoder_stem=cifar`): `conv1` is replaced by a  $3 \times 3$  stride-1 conv and `maxpool` is removed.
- **ImageNet stem** (`encoder_stem=imagenet`): keep the default  $7 \times 7$  stride-2 conv and `maxpool`.

**Token mode (used in all shown configs).** With `encoder_mode=tokens`, we expose an intermediate feature map at a chosen ResNet layer (`token_layer` in `{layer2, layer3, layer4}`), project its channels with a  $1 \times 1$  conv to `token_d_f`, optionally pool to a fixed spatial grid (`token_hw`), then flatten.

Concretely, if the token feature map has shape `[B, token_d_f, h, w]`, the flattened representation is

$$z \in \mathbb{R}^{B \times (hw \text{ token\_d\_f})}.$$

This is why `embed_dim` must match `hw token_d_f`:

- CIFAR100: `layer3` naturally yields an  $8 \times 8$  map, and with `token_d_f=32` we get  $8 \cdot 8 \cdot 32 = 2048$ .
- ImageNet: `layer3` yields  $14 \times 14$  pre-pool; we set `token_hw=8` so adaptive pooling yields  $8 \times 8$ , again giving 2048.

**Projector.** We support either an MLP projector or an identity projector. In MV-HJEPA we *require* `projector_type=identity` and enforce it in code, because we interpret the representation channels as structured phase-space coordinates and do not want a learned MLP to arbitrarily mix them.

**Phase-space split:**  $z = [q; p]$ . In MV-HJEPA we require an even representation dimension  $K = 2d$ , and interpret:

$$z = \begin{bmatrix} q \\ p \end{bmatrix} \in \mathbb{R}^{2d}, \quad q \in \mathbb{R}^d, p \in \mathbb{R}^d.$$

This split is implemented *channel-wise per token* in the encoder when `split_qp=true`: the token channel dimension `token_d_f` is split into equal halves (first half  $\rightarrow q$ , second half  $\rightarrow p$ ) before flattening and concatenation.

## F.5 Hamiltonian flow predictor (MV-HJEPA)

**Hamiltonian dynamics.** We predict one view’s state from another by integrating Hamiltonian dynamics in latent phase space. Given a Hamiltonian  $H(q, p)$ , the vector field is:

$$\frac{dq}{dt} = \frac{\partial H}{\partial p}, \quad \frac{dp}{dt} = -\frac{\partial H}{\partial q}.$$

In code,  $\partial H/\partial q$  and  $\partial H/\partial p$  are obtained via automatic differentiation (`torch.autograd.grad(create_graph=True)`), so gradients propagate through the integrator.

**Hamiltonian parameterizations.** `hamjepa/hamiltonian.py` supports:

1. **Quadratic:**  $H(q, p) = \frac{1}{2}(\|q\|^2 + \|p\|^2)$  (no learnable parameters).
2. **Learnable (residual MLP):**

$$H_\theta(q, p) = \frac{1}{2}(\|q\|^2 + \|p\|^2) + s f_\theta([q, p]),$$

where  $s$  (`residual_scale`) is a stabilizing residual multiplier.

3. **Separable (used for MV-HJEPA):**

$$H_\phi(q, p) = T(p) + V_\phi(q), \quad T(p) = \frac{1}{2}\|p\|^2, \quad V_\phi(q) = \frac{1}{2}\alpha\|q\|^2 + s f_\phi(q),$$

where  $\alpha$  (`base_coeff`) is a fixed quadratic base coefficient and  $s$  (`residual_scale`) is a residual scaling factor.

The separable form enables an explicit velocity-Verlet/leapfrog update that is symplectic.

**Residual-scale warmup.** In MV-HJEPA, we linearly warm up `residual_scale` over `residual_scale_warmup_epochs`. Early in training the potential is close to purely quadratic (stable), and the learned residual is introduced gradually.

**Step size and fp32 integration.** We integrate for `steps=S` steps with step size `dt` (fixed in MV-HJEPA; `learn_dt=false`). For mixed precision runs (bf16), we optionally do the dynamics computations in fp32 and cast back (`integrate_fp32=true`) to stabilize higher-order autodiff through the integrator.

## F.6 Symplectic integrators

We implement:

- **Symplectic Euler** for general  $H(q, p)$ .
- **Leapfrog / velocity-Verlet:**
  - a general variant using autodiff for  $\nabla_q H$  and  $\nabla_p H$
  - a specialized separable variant (used by MV-HJEPA when  $H = T + V$ ) using only  $\nabla V(q)$

For separable  $H(q, p) = \frac{1}{2}\|p\|^2 + V(q)$ , the specialized update is:

$$p_{1/2} = p - \frac{\Delta t}{2}\nabla V(q), \quad q \leftarrow q + \Delta t p_{1/2}, \quad p \leftarrow p_{1/2} - \frac{\Delta t}{2}\nabla V(q).$$

### F.7 MV-HJEPA prediction loss

Given two global views' states  $z_a = [q_a; p_a]$  and  $z_b = [q_b; p_b]$ , we predict:

$$\hat{z}_b = \text{Flow}_H(z_a; \Delta t, S),$$

and compute a MSE matching term either on  $q$  only or the full  $(q, p)$  state:

$$\mathcal{L}_{\text{match}} = \begin{cases} \text{MSE}(\hat{q}_b, q_b) + w_p \text{MSE}(\hat{p}_b, p_b) & (\text{match} = q) \\ \text{MSE}(\hat{z}_b, z_b) & (\text{match} = qp). \end{cases}$$

We typically stop-gradient the target branch (`detach_target=true`) to prevent trivial collapse.

Optionally, we add an energy-consistency term that encourages the flow to preserve the input energy:

$$\mathcal{L}_{\text{energy}} = \text{MSE}(H(q_a, p_a), H(\hat{q}_b, \hat{p}_b)),$$

and the full prediction loss is:

$$\mathcal{L}_{\text{pred}} = \mathcal{L}_{\text{match}} + \lambda_E \mathcal{L}_{\text{energy}}.$$

**Bidirectional training.** If enabled, we symmetrize by predicting in both directions.

$$\mathcal{L}_{\text{pred}} \leftarrow \frac{1}{2} (\mathcal{L}_{\text{pred}}(z_0, z_1) + \mathcal{L}_{\text{pred}}(z_1, z_0)).$$

In the most physically consistent variant, the reverse direction uses reverse-time integration (negated  $\Delta t$ ), which is supported by the predictor's `direction` flag.

### F.8 Regularizers (applied across all views)

We compute regularizers on the concatenation of all views' states:

$$z_{\text{all}} \in \mathbb{R}^{(VB) \times 2d}.$$

**Phase-space energy budget (scale control).** We stabilize scale in fixed units by enforcing per-coordinate second moments:

$$\mathcal{L}_{\text{budget}} = (\mathbb{E}[q^2] - q_{\text{tgt}})^2 + (\mathbb{E}[p^2] - p_{\text{tgt}})^2,$$

where expectations are taken over batch and coordinates in fp32 and can be Distributed Data Parallel (DDP)-synchronized.

**Variance floor (anti-collapse).** Let  $\sigma_i$  be the batch standard deviation of dimension  $i$  (fp32 stats). We apply:

$$\mathcal{L}_{\text{var}} = \frac{1}{d} \sum_{i=1}^d \max(0, \sigma_{\text{min}} - \sigma_i)^2,$$

typically on  $q$  and optionally on  $p$  depending on the experiment.

**Projected log-determinant floor (spectral diversity).** We enforce a lower bound on the log-determinant of a randomly projected covariance. Given  $x \in \mathbb{R}^{B \times d}$ , sample an orthonormal projection  $R \in \mathbb{R}^{d \times k}$ , compute  $y = (x - \bar{x})R$ , then:

$$C = \text{Cov}(y) + \varepsilon I, \quad \mathcal{L}_{\log \det} = \max\left(0, \tau - \frac{1}{k} \log \det(C)\right)^2.$$

We optionally add constraints on the participation ratio  $\text{PR} = \text{tr}(C)^2 / \text{tr}(C^2)$  and the top-eigenvalue fraction  $\lambda_{\text{max}} / \text{tr}(C)$ .

**Mean penalty.** We penalize non-zero feature means using the squared mean (fp32):

$$\mathcal{L}_{\text{mean}} \propto \|\mathbb{E}[z]\|_2^2.$$

## F.9 Training step summary

**MV-HJEPA.** At each step:

1. Build  $V$  views per image, concatenate them, and compute  $z_{\text{views}} \in \mathbb{R}^{V \times B \times 2d}$ .
2. Select the two global views  $(z_0, z_1)$  and compute  $\mathcal{L}_{\text{pred}}$  via Hamiltonian flow prediction.
3. Compute  $\mathcal{L}_{\text{budget}}, \mathcal{L}_{\text{var}}, \mathcal{L}_{\log \det}$ , and  $\mathcal{L}_{\text{mean}}$  on all views.
4. Optimize encoder + (identity) projector + predictor parameters with AdamW, optional gradient clipping, and cosine LR schedule with warmup.

**Baseline (LeJEPA + SIGReg/HamSIGReg).** If `hjepa` is absent:

1. Compute  $z_{\text{views}}$  as above.
2. Apply LeJEPA prediction loss: all views match the per-sample mean of global views.
3. Add a distributional regularizer (e.g. SIGReg) with weight `lambda_reg`.
4. If the regularizer includes a learnable metric  $H$ , optionally update  $H$  on a slower/periodic schedule.

## F.10 Algorithms

**Notation.** Let  $V$  be the number of augmented views per image,  $B$  the batch size, and  $K$  the representation dimension. In MV-HJEPA we enforce  $K = 2d$  and interpret each representation as a phase-space state  $z = [q; p] \in \mathbb{R}^{2d}$  with  $q, p \in \mathbb{R}^d$  (channel-wise split, `split_qp=true`). We write  $\text{concat}_v, x^{(v)}$  for concatenation of views along the batch dimension, and `reshape` for a view/batch reshape with the same underlying memory order as the implementation.

---

**Algorithm 1** Multi-crop view generation (used by `CIFAR100MultiCrop` and `ImageNetMultiCrop`)

---

**Input:** Image  $I$ , multi-crop config:  $(V_g, V_\ell)$ , output size  $s$ , scales  $(\alpha_g, \beta_g)$  and  $(\alpha_\ell, \beta_\ell)$

**Output:** List of views  $\{x^{(v)}\}_{v=1}^V$  where  $V = V_g + V_\ell$

- 1: Initialize empty list `views`  $\leftarrow []$
  - 2: **for**  $i = 1$  to  $V_g$  **do**
  - 3:      $x \leftarrow \text{Augment}(I; \text{RandomResizedCrop}(s, \text{scale} = [\alpha_g, \beta_g]), \text{HFlip}, \text{CJ}, \text{Gray}, \text{Blur}, \text{Solarize})$
  - 4:     Append  $x$  to `views`
  - 5: **end for**
  - 6: **for**  $i = 1$  to  $V_\ell$  **do**
  - 7:      $x \leftarrow \text{Augment}(I; \text{RandomResizedCrop}(s, \text{scale} = [\alpha_\ell, \beta_\ell]), \text{HFlip}, \text{CJ}, \text{Gray}, \text{Blur}, \text{Solarize})$
  - 8:     Append  $x$  to `views`
  - 9: **end for**
  - 10: **return** `views`
- 

**Implementation note (dataset-specific):** CIFAR views are produced as float tensors with normalization applied in the dataset pipeline; ImageNet views are emitted as compact `uint8` tensors (via `PILToTensor`) and normalized on-device in the training loop.

---

**Algorithm 2** ResNet token encoder forward pass (token mode, optional  $q/p$  split)

---

**Input:** Image batch  $x \in \mathbb{R}^{B \times 3 \times H \times W}$ , ResNet stem+layers, token layer  $\ell \in \{\text{layer2}, \text{layer3}, \text{layer4}\}$ , channel projection to  $d_f$ , optional pooling to `token_hw = h = w`, `split_qp` flag

**Output:** Representation  $z \in \mathbb{R}^{B \times K}$  where  $K = h \cdot w \cdot d_f$

- 1:  $u \leftarrow \text{stem}(x)$
- 2:  $u \leftarrow \text{layer1}(u)$
- 3:  $u \leftarrow \text{layer2}(u)$ ; set `fmap`  $\leftarrow u$  if  $\ell = \text{layer2}$
- 4:  $u \leftarrow \text{layer3}(u)$ ; set `fmap`  $\leftarrow u$  if  $\ell = \text{layer3}$

```

5:  $u \leftarrow \text{layer4}(u)$ ; set fmap  $\leftarrow u$  if  $\ell = \text{layer4}$ 
6: if token_hw is set then
7:   fmap  $\leftarrow \text{AdaptiveAvgPool2d}(\text{fmap}, (h, w))$ 
8: end if
9:  $t \leftarrow \text{Conv1} \times 1 + \text{BN}(\text{fmap}) \in \mathbb{R}^{B \times d_f \times h \times w}$ 
10:  $t \leftarrow \text{permute}(t) \in \mathbb{R}^{B \times h \times w \times d_f}$ 
11: if split_qp = false then
12:    $z \leftarrow \text{flatten}(t) \in \mathbb{R}^{B \times (hwd_f)}$ 
13: else
14:   Split channels:  $t \mapsto (t_q, t_p)$  with  $t_q, t_p \in \mathbb{R}^{B \times h \times w \times (d_f/2)}$ 
15:    $q \leftarrow \text{flatten}(t_q) \in \mathbb{R}^{B \times (hw(d_f/2))}$ ;  $p \leftarrow \text{flatten}(t_p) \in \mathbb{R}^{B \times (hw(d_f/2))}$ 
16:    $z \leftarrow [q; p] \in \mathbb{R}^{B \times (hwd_f)}$ 
17: end if
18: return  $z$ 

```

---

**Algorithm 3** MV-HJEPA training step (matches train\*\_hamjepa.py when hjepa: is present)

**Input:** Views  $\{x^{(v)}\}_{v=1}^V$ , encoder  $E$ , projector  $P$  (identity for MV-HJEPA), predictor  $\text{Flow}_H$ , loss/regularizer weights  $\lambda$ .

**Input:** MV-HJEPA requires split\_qp=true and  $K = 2d$

```

1:  $x_{\text{cat}} \leftarrow \text{concat}_v x^{(v)} \in \mathbb{R}^{(VB) \times C \times H \times W}$ 
2:  $z_{\text{cat}} \leftarrow P(E(x_{\text{cat}})) \in \mathbb{R}^{(VB) \times 2d}$ 
3:  $z_{\text{views}} \leftarrow \text{reshape}(z_{\text{cat}}) \in \mathbb{R}^{V \times B \times 2d}$ 
4:  $z_0 \leftarrow z_{\text{views}}[0]$ ,  $z_1 \leftarrow z_{\text{views}}[1]$ 
5:  $\mathcal{L}_{\text{pred}} \leftarrow \text{HamConsistency}(z_0, z_1)$ 
6: if bidirectional then
7:    $\mathcal{L}_{\text{pred}} \leftarrow \frac{1}{2} (\mathcal{L}_{\text{pred}} + \text{HamConsistency}(z_1, z_0))$ 
8: end if
9:  $z_{\text{all}} \leftarrow z_{\text{views}}.\text{reshape}(VB, 2d)$ 
10: Split  $z_{\text{all}} \mapsto (q_{\text{all}}, p_{\text{all}})$  along the last dimension
11:  $\mathcal{L}_{\text{budget}} \leftarrow \text{EnergyBudget}(z_{\text{all}})$ 
12:  $\mathcal{L}_{\text{var}} \leftarrow \text{VarFloor}(q_{\text{all}}) + \text{VarFloor}(p_{\text{all}})$  if enabled in that script)
13:  $\mathcal{L}_{\text{log det}} \leftarrow \text{LogDetFloor}(q_{\text{all}}) + \text{LogDetFloor}(p_{\text{all}})$ 
14:  $\mathcal{L}_{\text{mean}} \leftarrow \text{mean}(z_{\text{all}})^{\odot 2}$  averaged over dimensions  $\triangleright$  matches mean().square().mean()
15:  $\mathcal{L} \leftarrow \mathcal{L}_{\text{pred}} + \lambda_{\text{budget}} \mathcal{L}_{\text{budget}} + \lambda_{\text{var}} \mathcal{L}_{\text{var}} + \lambda_{\text{log det}} \mathcal{L}_{\text{log det}} + \lambda_{\text{mean}} \mathcal{L}_{\text{mean}}$ 
16: Update parameters of  $\{E, P, \text{Flow}_H\}$  with AdamW; optionally clip gradients and step LR schedule

```

---

**Algorithm 4** Hamiltonian Consistency loss (HamiltonianConsistencyLoss)

**Input:** States  $z_a, z_b \in \mathbb{R}^{B \times 2d}$ , predictor  $\text{Flow}_H$ , options: detach\_target, match  $\in \{q, qp\}$ , p\_weight, energy\_weight, bidirectional

**Output:** Scalar loss  $\mathcal{L}$

```

1:  $\hat{z}_{a \rightarrow b} \leftarrow \text{Flow}_H(z_a; \text{direction} = +1)$ 
2:  $z_b^* \leftarrow z_b$  if not detach_target else stopgrad( $z_b$ )
3: if match=qp then
4:    $\ell_{a \rightarrow b} \leftarrow \text{MSE}(\hat{z}_{a \rightarrow b}, z_b^*)$ 
5: else  $\triangleright$  match=q
6:    $\ell_{a \rightarrow b} \leftarrow \text{MSE}(\hat{z}_{a \rightarrow b}[:, :d], z_b^*[:, :d])$ 
7:   if p_weight > 0 then
8:      $\ell_{a \rightarrow b} \leftarrow \ell_{a \rightarrow b} + \text{p\_weight} \cdot \text{MSE}(\hat{z}_{a \rightarrow b}[:, d:], z_b^*[:, d:])$ 
9:   end if
10: end if
11: if energy_weight > 0 then
12:   Split  $z_a \mapsto (q_a, p_a)$  and  $\hat{z}_{a \rightarrow b} \mapsto (\hat{q}, \hat{p})$ 
13:    $H_a \leftarrow \text{stopgrad}(H(q_a, p_a))$ ;  $H_{\hat{z}} \leftarrow H(\hat{q}, \hat{p})$ 
14:    $\ell_{a \rightarrow b} \leftarrow \ell_{a \rightarrow b} + \text{energy\_weight} \cdot \text{MSE}(H_{\hat{z}}, H_a)$ 
15: end if
16:  $\mathcal{L} \leftarrow \ell_{a \rightarrow b}$ 

```

---

```

17: if bidirectional then
18:   Compute  $\ell_{b \rightarrow a}$  identically using direction = -1 and target  $z_a$  (optionally detached)
19:    $\mathcal{L} \leftarrow \frac{1}{2}(\ell_{a \rightarrow b} + \ell_{b \rightarrow a})$ 
20: end if
21: return  $\mathcal{L}$ 

```

---

**Algorithm 5** Hamiltonian Flow Predictor (forward pass, HamiltonianFlowPredictor)

---

```

Input: State  $z_0 \in \mathbb{R}^{\dots \times 2d}$ , Hamiltonian module  $H$ , method, steps  $S$ , base step size  $\Delta t > 0$ , direction
 $s \in \{+1, -1\}$ , integrate_fp32, learn_dt
Output: State  $z_T \in \mathbb{R}^{\dots \times 2d}$ 
1: Split  $z_0 \mapsto (q_0, p_0)$ 
2:  $\Delta t \leftarrow s \cdot \Delta t$ ; if learn_dt, set  $\Delta t \leftarrow s \cdot \text{softplus}(\text{raw\_dt})$ 
3: if integrate_fp32 enabled and dtype(z_0) \in \{fp16, bf16\} then
4:   Cast  $(q_0, p_0)$  to fp32
5: end if
6: if  $H$  is separable and method is leapfrog then
7:    $(q_T, p_T) \leftarrow \text{IntegrateSeparableLeapfrog}(V_\phi, q_0, p_0, \Delta t, S)$ 
8: else
9:    $(q_T, p_T) \leftarrow \text{IntegrateHamiltonian}(H, q_0, p_0, \Delta t, S, \text{method})$ 
10: end if
11:  $z_T \leftarrow [q_T; p_T]$ 
12: if integrate_fp32 enabled and original dtype was bf16/fp16 then
13:   Cast  $z_T$  back to the original dtype
14: end if
15: return  $z_T$ 

```

---

**Algorithm 6** Symplectic integration routines (as in hamjepa/integrators.py)

---

```

Input: General Hamiltonian  $H(q, p)$  or separable potential  $V(q)$ , initial  $(q, p)$ , step size  $\Delta t$ , steps
 $S$ , method  $\in \{\text{leapfrog}, \text{symplectic\_euler}\}$ 
Output: Final  $(q, p)$  after  $S$  steps
1: function INTEGRATEHAMILTONIAN( $H, q, p, \Delta t, S, \text{method}$ )
2:   for  $n = 1$  to  $S$  do
3:     if method = symplectic_euler then
4:        $p \leftarrow p - \Delta t \nabla_q H(q, p)$ 
5:        $q \leftarrow q + \Delta t \nabla_p H(q, p)$  ▷  $\nabla_p$  uses updated  $p$ 
6:     else ▷ method = leapfrog (velocity Verlet)
7:        $p_{1/2} \leftarrow p - \frac{\Delta t}{2} \nabla_q H(q, p)$ 
8:        $q \leftarrow q + \Delta t \nabla_p H(q, p_{1/2})$ 
9:        $p \leftarrow p_{1/2} - \frac{\Delta t}{2} \nabla_q H(q, p_{1/2})$ 
10:    end if
11:  end for
12:  return  $(q, p)$ 
13: end function
14: function INTEGRATESEPARABLELEAPFROG( $V, q, p, \Delta t, S$ )
15:  for  $n = 1$  to  $S$  do
16:     $p_{1/2} \leftarrow p - \frac{\Delta t}{2} \nabla_q V(q)$ 
17:     $q \leftarrow q + \Delta t \nabla_p V(q, p_{1/2})$ 
18:     $p \leftarrow p_{1/2} - \frac{\Delta t}{2} \nabla_q V(q)$  ▷  $\nabla_q V$  uses updated  $q$ 
19:  end for
20:  return  $(q, p)$ 
21: end function

```

---

**Algorithm 7** Phase-space energy budget regularizer (PhaseSpaceEnergyBudget)

---

```

Input: States  $z \in \mathbb{R}^{\dots \times 2d}$ , targets  $(q_{\text{tgt}}, p_{\text{tgt}})$ , ddp_sync
Output: Scalar loss  $\mathcal{L}_{\text{budget}}$ 
1: Flatten  $z \rightarrow z_f \in \mathbb{R}^{N \times 2d}$  and cast to fp32

```

---



---

```

2: Split  $z_f \mapsto (q, p)$  with  $q, p \in \mathbb{R}^{N \times d}$ 
3:  $q2\_sum \leftarrow \sum q^{\odot 2}$ ,  $p2\_sum \leftarrow \sum p^{\odot 2}$ ,  $count \leftarrow Nd$ 
4: if ddp_sync and DDP initialized then
5:   All-reduce (SUM)  $q2\_sum, p2\_sum$ , and  $count$ 
6: end if
7:  $q2\_mu \leftarrow q2\_sum / count$ ;  $p2\_mu \leftarrow p2\_sum / count$ 
8:  $\mathcal{L}_{budget} \leftarrow (q2\_mu - q_{tgt})^2 + (p2\_mu - p_{tgt})^2$ 
9: return  $\mathcal{L}_{budget}$ 

```

---



---

**Algorithm 8** Variance floor regularizer (VarianceFloor)

---

**Input:** Features  $x \in \mathbb{R}^{N \times d}$ , std floor  $\sigma_{\min}, \varepsilon, \text{ddp\_sync}$   
**Output:** Scalar loss  $\mathcal{L}_{\text{var}}$

```

1: Cast  $x$  to fp32; if  $N < 2$  return 0
2: Compute sufficient stats:  $s_1 \leftarrow \sum_n x_n$ ,  $s_2 \leftarrow \sum_n x_n^{\odot 2}$ , and  $n \leftarrow N$ 
3: if ddp_sync and DDP initialized then
4:   All-reduce (SUM)  $s_1, s_2$ , and  $n$ 
5: end if
6:  $\mu \leftarrow s_1 / n$ ;  $\text{var} \leftarrow s_2 / n - \mu^{\odot 2}$ ;  $\sigma \leftarrow \sqrt{\max(\text{var}, 0)} + \varepsilon$ 
7:  $\mathcal{L}_{\text{var}} \leftarrow \frac{1}{d} \sum_{i=1}^d \text{ReLU}(\sigma_{\min} - \sigma_i)^2$ 
8: return  $\mathcal{L}_{\text{var}}$ 

```

---



---

**Algorithm 9** Projected log-det floor (ProjectedLogDetFloor)

---

**Input:** Features  $x \in \mathbb{R}^{B \times D}$ , projection dim  $k$ , log-det floor  $\ell_{\min}, \varepsilon$ , refresh interval  $r$ , optional `pr_norm_floor` and `eigmax_frac_ceiling`, `ddp_sync`  
**Output:** Scalar loss  $\mathcal{L}_{\log \det}$

```

1: Cast  $x$  to fp32; if  $B < 2$  return 0
2:  $k \leftarrow \min(k, D, B - 1)$ 
3: if need resample (first call / device change / shape change / step mod  $r = 0$ ) then
4:   Sample  $R \sim \mathcal{N}(0, 1)^{D \times k}$  and orthonormalize columns via QR:  $R \leftarrow \text{qr}(R)$ 
5: end if
6: Center and project:  $x_c \leftarrow x - \text{mean}(x)$ ;  $y \leftarrow x_c R \in \mathbb{R}^{B \times k}$ 
7: Compute sufficient stats:  $\text{sum}_y \leftarrow \sum_b y_b$ ,  $\text{sum}_{yy} \leftarrow y^\top y$ ,  $n \leftarrow B$ 
8: if ddp_sync and DDP initialized then
9:   All-reduce (SUM)  $\text{sum}_y, \text{sum}_{yy}$ , and  $n$ 
10: end if
11:  $n \leftarrow \max(n, 2)$ ;  $\mu_y \leftarrow \text{sum}_y / n$ 
12:  $\Sigma \leftarrow \frac{\text{sum}_{yy} - n \cdot (\mu_y \mu_y^\top)}{n - 1}$ ;  $\Sigma \leftarrow \frac{1}{2}(\Sigma + \Sigma^\top) + \varepsilon I$ 
13:  $\ell \leftarrow \frac{1}{k} \log \det(\Sigma)$  ▷ implemented via slogdet
14:  $\mathcal{L}_{\log \det} \leftarrow \text{ReLU}(\ell_{\min} - \ell)^2$ 
15: Compute PR =  $\frac{\text{tr}(\Sigma)^2}{\text{tr}(\Sigma^2)}$ ,  $\text{pr\_norm} = \text{PR} / k$ , and  $\text{eigmax\_frac} = \lambda_{\max} / \text{tr}(\Sigma)$ 
16: if pr_norm_floor is set then
17:    $\mathcal{L}_{\log \det} \leftarrow \mathcal{L}_{\log \det} + \text{ReLU}(\text{pr\_norm\_floor} - \text{pr\_norm})^2$ 
18: end if
19: if eigmax_frac_ceiling is set then
20:    $\mathcal{L}_{\log \det} \leftarrow \mathcal{L}_{\log \det} + \text{ReLU}(\text{eigmax\_frac} - \text{eigmax\_frac\_ceiling})^2$ 
21: end if
22: return  $\mathcal{L}_{\log \det}$ 

```

---



---

**Algorithm 10** SIGReg forward pass (random slicing + Epps–Pulley statistic)

---

**Input:** Batch  $z \in \mathbb{R}^{\dots \times N \times D}$ , slices  $K$ , knots  $t_1, \dots, t_T$  (with weights  $w$ ), refresh interval  $r$ , `ddp_sync`  
**Output:** Scalar statistic  $S(z)$  (mean-reduced in our configs)

```

1: (Slicing) If step mod  $r = 0$ , sample  $A \in \mathbb{R}^{D \times K}$  with i.i.d.  $\mathcal{N}(0, 1)$  columns and normalize each column to unit norm

```

- 2: **if** `ddp_sync` and DDP initialized **then**
- 3:   Ensure all ranks share the same sampling seed for  $A$  (broadcast seed from rank 0)
- 4: **end if**
- 5: Project:  $y \leftarrow zA \in \mathbb{R}^{\dots \times N \times K}$
- 6: (**Epps–Pulley**) Compute empirical CF on each slice:
- 7:    $\hat{c}(t) = \frac{1}{N} \sum_n \cos(t y_n)$ ,  $\hat{s}(t) = \frac{1}{N} \sum_n \sin(t y_n)$  (optionally globally averaged via all-reduce if `ddp_sync`)
- 8:   Target CF for  $\mathcal{N}(0, 1)$  is  $\phi(t) = e^{-t^2/2}$
- 9:    $S_k \leftarrow N \sum_{j=1}^T w_j \left[ (\hat{c}(t_j) - \phi(t_j))^2 + \hat{s}(t_j)^2 \right]$  for each slice  $k$
- 10: Reduce over slices (and leading dims) by mean:  $S(z) \leftarrow \text{mean}_k(S_k)$
- 11: **return**  $S(z)$

**Algorithm 11** LeJEPA baseline step with SIGReg regularization (non-MV branch in `train*_hamjepa.py`)

- Input:** Views  $\{x^{(v)}\}_{v=1}^V$ , encoder  $E$ , projector  $P$ , number of global views  $V_g$ , regularizer  $\mathcal{R}$  (SIGReg), weight  $\lambda_{\text{reg}}$
- 1:  $x_{\text{cat}} \leftarrow \text{concat}_v x^{(v)}$
  - 2:  $z_{\text{cat}} \leftarrow P(E(x_{\text{cat}})) \in \mathbb{R}^{(VB) \times D}$
  - 3:  $z_{\text{views}} \leftarrow \text{reshape}(z_{\text{cat}}) \in \mathbb{R}^{V \times B \times D}$
  - 4:  $\bar{z} \leftarrow \frac{1}{V_g} \sum_{v=1}^{V_g} z_{\text{views}}[v] \in \mathbb{R}^{B \times D}$  ▷ mean of global views
  - 5:  $\mathcal{L}_{\text{pred}} \leftarrow \frac{1}{2} \text{mean}(\|z_{\text{views}} - \bar{z}\|_2^2)$  ▷ matches `lejepa_prediction_loss`
  - 6:  $\mathcal{L}_{\text{reg}} \leftarrow \mathcal{R}(z_{\text{views}})$  ▷ SIGReg expects shape  $(\dots, N, D)$
  - 7:  $\mathcal{L} \leftarrow \mathcal{L}_{\text{pred}} + \lambda_{\text{reg}} \mathcal{L}_{\text{reg}}$  ▷ spectral term omitted here (zero in our SIGReg configs)
  - 8: Update  $\{E, P\}$  with AdamW; optionally step LR schedule and log diagnostics

## F.11 YAML Configuration Knobs

The repository is fully config-driven: the training scripts read a YAML file and route into either (i) MV-HJEPA mode when the `hjepa:` stanza is present (and `split_qp=true`), or (ii) the LeJEPA+regularizer baseline when `hjepa:` is absent (e.g. `regularizer.type=sigreg`). Below we document every key appearing in the provided configs, exactly as it is consumed by the code. We keep `seed=42` for reproducibility across runs.

### F.11.1 Data (`data:`)

- `root`: Dataset root path passed to CIFAR100 / ImageFolder loader.
- `batch_size`: DataLoader batch size (`batch_size=batch_size`). We use larger batches on CIFAR (512) and smaller on ImageNet (256) to balance GPU memory and throughput.
- `num_workers`: DataLoader worker count. Higher values improve input pipeline throughput when CPU-bound.
- `drop_last`: If true, drops the last incomplete batch. This avoids smaller last batches, which can destabilize batch statistics and covariance-based regularizers (and helps DDP batch-size consistency).
- `pin_memory` (ImageNet configs): Enables pinned host memory to speed CPU→GPU transfers.
- `persistent_workers` (ImageNet configs): Keeps workers alive across epochs to reduce worker spin-up overhead.
- `prefetch_factor` (ImageNet configs): Worker prefetch depth; increases overlap between CPU augmentation and GPU training.
- `num_global_views`, `num_local_views`: Multi-crop configuration. In all provided runs we set two global views and no local views (2/0), matching the two-view training objective in both MV-HJEPA and the LeJEPA baseline.
- `out_size` (ImageNet configs): Output crop resolution for RandomResizedCrop. We use 224 (standard ImageNet scale).

- `global_scale`, `local_scale` (ImageNet configs): Scale ranges for global/local crops. Only global crops are used when `num_local_views=0`.
- *CIFAR note*: the CIFAR YAMLs omit `out_size/global_scale/local_scale`, so the dataset defaults are used (`out_size=32`, `global_scale=(0.3,1.0)`, `local_scale=(0.05,0.3)`).

### F.11.2 Model (model:)

- `encoder_mode`: `global` uses GAP (global average pooling)+FC; `tokens` exposes an intermediate feature map and flattens it into tokens. All provided configs use `tokens`.
- `encoder_stem`: `cifar` modifies ResNet-18 stem ( $3 \times 3$  stride 1, no maxpool) for  $32 \times 32$  inputs; `imagenet` keeps the default  $7 \times 7$  stride 2 + maxpool stem.
- `token_layer`: Which ResNet stage to expose as the token grid (`layer2/layer3/layer4`). We use `layer3`, giving an  $8 \times 8$  grid on CIFAR and a  $14 \times 14$  grid on ImageNet before any optional pooling.
- `token_d_f`: Number of channels after the  $1 \times 1$  token projection (Conv $1 \times 1$ +BN). In token mode, the representation dimension is  $K = h \cdot w \cdot \text{token\_d\_f}$ .
- `token_hw` (ImageNet configs): Optional adaptive pooling size for the token grid. We set `token_hw=8` on ImageNet so that with `token_d_f=32` we obtain  $K = 8 \cdot 8 \cdot 32 = 2048$  (matching `embed_dim`).
- `embed_dim`: Output dimension  $K$  of the encoder in token mode. For our settings this is tied to the token grid geometry (e.g.  $8 \cdot 8 \cdot 32 = 2048$ ).
- `proj_hidden`, `proj_out`: Hidden/output sizes for the optional MLP projector. These are read from the YAML but are only used when `projector_type=mlp`.
- `projector_type`: `identity` returns  $z$  unchanged; `mlp` applies `MLPProjector`. MV-HJEPA requires `identity` so the channel-wise  $q/p$  semantics are preserved.
- `split_qp`: If true, the token channels are split into  $(q, p)$  halves per token and concatenated, enforcing  $K = 2d$  and enabling the phase-space interpretation required by MV-HJEPA.

### F.11.3 MV-HJEPA predictor (hjepa:)

(Only present in `*_hjepa_mv.yaml` configs.)

- `hamiltonian`: Choice of Hamiltonian parameterization. We use `separable`, i.e.  $H(q, p) = \frac{1}{2} \|p\|^2 + V_\phi(q)$ , to enable explicit symplectic leapfrog integration.
- `method`: Integrator choice. We use `leapfrog` (velocity Verlet), implemented in `integrate_separable_leapfrog` for separable  $H$ .
- `steps`: Number of integrator steps  $S$  per forward pass. We use 2 to keep compute low while still giving a nontrivial flow.
- `dt`: Fixed step size  $\Delta t$ . Used as a constant buffer when `learn_dt=false`.
- `learn_dt`: If true,  $\Delta t$  becomes learnable via a softplus parameterization. MV-HJEPA disables this (`false`) and the training script explicitly rejects learnable- $dt$  to avoid degenerate solutions (“dt-collapse”).
- `hidden_dim`, `depth`: MLP size/depth used inside the Hamiltonian residual network (for  $V_\phi$  in the separable case).
- `residual_scale`: Multiplier on the Hamiltonian residual output. This is a stability knob: the code is designed so the Hamiltonian has a quadratic base plus a small learned residual.
- `residual_scale_warmup_epochs`: Linearly ramps `residual_scale` from 0 to its target value over the first epochs (implemented by overwriting `predictor.H.residual_scale` each epoch).
- `base_coeff`: Coefficient on the quadratic base potential term in  $V(q)$  (i.e.  $0.5 \text{base\_coeff} \|q\|^2$ ). Keeping this nonzero prevents the “trivial potential” loophole where dynamics can collapse.
- `integrate_fp32`: If true, the predictor casts  $z$  to fp32 during integration when training in bf16/fp16, improving numerical stability of gradient-based integration.

#### F.11.4 MV-HJEPA loss (loss:)

- `match`: Which part of the state to match in the consistency loss: `q` matches positions only (optionally with a small `p` penalty), while `qp` matches the full state.
- `p_weight`: Only used when `match=q`. Adds an auxiliary MSE on `p` with weight `p_weight`.
- `detach_target`: If true, the target branch is detached in the prediction loss (safer default to prevent the target moving to satisfy the predictor).
- `energy_weight`: Optional extra term matching  $H(z)$  before/after the flow. Set to 0.0 in all provided configs (disabled).
- `bidirectional`: If true, averages forward and backward consistency ( $z_0 \rightarrow z_1$  and  $z_1 \rightarrow z_0$ ). In the ImageNet training script this averaging is done explicitly in the loop; in the CIFAR script it can be handled inside the loss module.

#### F.11.5 MV-HJEPA anti-collapse regularizers (regularizer:)

(These are the *phase-space* regularizers used in the MV-HJEPA branch; they are not the SIGReg baseline.)

- `q_per_dim_target`, `p_per_dim_target`: Targets for the phase-space energy budget: they control the desired per-dimension mean-square magnitude of `q` and `p`.
- `q_std_floor`: Per-dimension standard deviation floor used by `VarianceFloor` on `q` (and on `p` in the CIFAR MV script; ImageNet MV applies the variance floor to `q` only).
- `ddp_sync`: If true and DDP is initialized, the sufficient statistics for the budget/variance/logdet terms are aggregated across ranks using all-reduce. This makes the regularizers behave as if computed on the global batch.
- `q_logdet_proj_dim`, `p_logdet_proj_dim`: Projection dimension  $k$  for the log-det regularizer on `q` and `p`.
- `q_logdet_floor`, `p_logdet_floor`: Minimum allowed log-determinant per projected dimension (a volume floor) used by `ProjectedLogDetFloor`.
- `q_logdet_eps`, `p_logdet_eps`: Diagonal jitter  $\epsilon I$  added to the covariance before computing `slogdet`.
- `q_logdet_refresh_interval`, `p_logdet_refresh_interval`: How often the random projection matrix is resampled (larger values reduce overhead and noise by reusing projections).
- `q_pr_norm_floor`, `p_pr_norm_floor`: Optional lower bounds on normalized participation ratio  $PR/k$  (encourages higher effective rank).
- `q_eigmax_frac_ceiling`, `p_eigmax_frac_ceiling`: Optional upper bounds on  $\lambda_{\max}/\text{tr}(\Sigma)$  to prevent a single dominant direction.

#### F.11.6 Training (train:)

- `epochs`: Total training epochs.
- `lr`: Base AdamW learning rate for encoder/projector (and predictor in CIFAR MV).
- `h_lr` (ImageNet MV config): Separate learning rate used specifically for the Hamiltonian parameters inside the predictor (`predictor.H.parameters()`); the ImageNet training script builds a two-group optimizer when these parameters exist.
- `weight_decay`: AdamW weight decay for the main optimizer.
- `warmup_epochs`: Warmup duration used by the linear warmup + cosine decay scheduler (when enabled by the script).
- `min_lr_ratio`: Sets  $\eta_{\min} = \text{lr} \cdot \text{min\_lr\_ratio}$  for cosine annealing.
- `precision`: Mixed precision mode. `bf16` enables CUDA autocast `bf16` in training.
- `ckpt_dir`: Output directory for checkpoints.
- `checkpoint_every` (ImageNet configs): Save checkpoints every  $k$  epochs (ImageNet script only).

- `grad_clip`: If  $> 0$ , applies global-norm gradient clipping (`clip_grad_norm_`).
- `log_every`: Print training diagnostics every `log_every` steps.
- `profile_timing`, `profile_every` (ImageNet MV config): Optional lightweight profiling of data time vs step time (only used in the ImageNet script).
- **MV-HJEPa loss weights**: `lambda_budget`, `lambda_var`, `lambda_logdet`, `lambda_mean` weight the corresponding regularizers in Algorithm 3.
- **SIGReg baseline weights**: `lambda_reg` is the coefficient on the SIGReg term in Algorithm 11.
- `h_update_interval`, `h_grad_clip` (SIGReg YAMLS): These knobs are parsed by the training scripts for the *learnable Hamiltonian regularizer* path (`regularizer.type=ham_sigreg` with learnable  $H$ ). In the provided SIGReg-only configs (`type=sigreg`), there are no  $H$  parameters, so these settings are effectively inert.